JACS
JOURNAL OF THE AMERICAN CHEMICAL SOCIETY
Article
pubs.acs.org/JACS

Influence of Pyrazolate vs *N*-Heterocyclic Carbene Ligands on the Slow Magnetic Relaxation of Homoleptic Trischelate Lanthanide(III) and Uranium(III) Complexes

Katie R. Meihaus,[†] Stefan G. Minasian,[‡] Wayne W. Lukens, Jr.,[‡] Stosh A. Kozimor,[§] David K. Shuh,[‡] Tolek Tyliszczak,[∥] and Jeffrey R. Long[†,*,⊥]

[†]Department of Chemistry, University of California, Berkeley, California 94720, United States
[‡]Chemical Sciences Division, Glenn T. Seaborg Center, Lawrence Berkeley National Laboratory, Berkeley, California 94720, United States
[∥]Advanced Light Source, Lawrence Berkeley National Laboratory, Berkeley, California 94720, United States
[§]Chemistry Division, Los Alamos National Laboratory, Los Alamos, New Mexico 87545, United States
[⊥]Materials Science Division, Lawrence Berkeley National Laboratory, Berkeley, California 94720, United States

Supporting Information

ABSTRACT: Two isostructural series of trigonal prismatic complexes, $M(Bp^{Me})_3$ and $M(Bc^{Me})_3$ (M = Y, Tb, Dy, Ho, Er, U; $[Bp^{Me}]^-$ = dihydrobis(methypyrazolyl)borate; $[Bc^{Me}]^-$ = dihydrobis(methylimidazolyl)borate) are synthesized and fully characterized to examine the influence of ligand donor strength on slow magnetic relaxation. Investigation of the dynamic magnetic properties reveals that the oblate electron density distributions of the Tb^{3+}, Dy^{3+}, and U^{3+} metal ions within the axial ligand field lead to slow relaxation upon application of a small dc magnetic field. Significantly, the magnetization relaxation is orders of magnitude slower for the *N*-heterocyclic carbene complexes, $M(Bc^{Me})_3$, than for the isomeric pyrazolate complexes, $M(Bp^{Me})_3$. Further, investigation of magnetically dilute samples containing 11−14 mol % of Tb^{3+}, Dy^{3+}, or U^{3+} within the corresponding Y^{3+} complex matrix reveals thermally activated relaxation is favored for the $M(Bc^{Me})_3$ complexes, even when dipolar interactions are largely absent. Notably, the dilute species $U(Bc^{Me})_3$ exhibits $U_{eff} \approx 33$ cm^{-1}, representing the highest barrier yet observed for a U^{3+} molecule demonstrating slow relaxation. Additional analysis through lanthanide XANES, X-band EPR, and ^{1}H NMR spectroscopies provides evidence that the origin of the slower relaxation derives from the greater magnetic anisotropy enforced within the strongly donating *N*-heterocyclic carbene coordination sphere. These results show that, like molecular symmetry, ligand-donating ability is a variable that can be controlled to the advantage of the synthetic chemist in the design of single-molecule magnets with enhanced relaxation barriers.

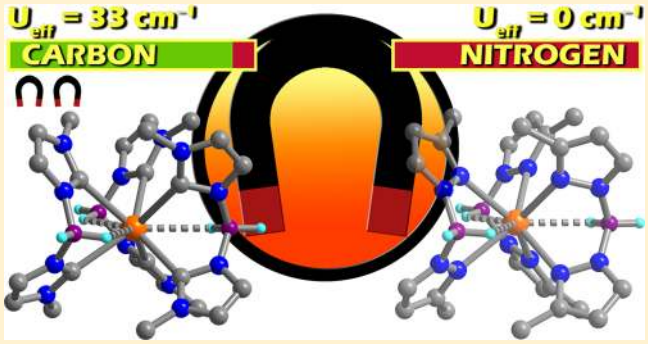

INTRODUCTION

The discovery of slow magnetic relaxation in f-element systems[1] led to a renaissance in the field of molecular magnetism. The lanthanides possess inherently large anisotropies and moments, arising from the near degeneracy of the magnetically active 4f orbitals, making them ideal for the design of single-molecule magnets with large relaxation barriers.[2] Likewise, with increased spin−orbit coupling, larger magnetic anisotropies, and greater radial extension of the 5f orbitals, the actinides are coming into their own as candidates for mononuclear and exchange-coupled single-molecule magnets.[3] Several recent approaches to the design of multinuclear f-element single-molecule magnets have proven highly successful, including coupling via radical ligands,[4] diamagnetic bridges[5] or cation−cation interactions,[3h] and oxo-bridged tetra- or pentanuclear clusters demonstrating large relaxation barriers arising from single-ion effects.[3h,6] However, for the lanthanides in particular, mononuclear complexes often display even longer relaxation times and larger spin-reversal barriers, deriving from single-ion anisotropy engineered through interaction with an appropriate crystal field.[7]

Alongside the remarkable synthetic progress has come the development of several ways of rationalizing slow magnetic relaxation. *Ab initio* calculations have been used extensively in the study of mononuclear 4f element complexes[6b,8] and provide valuable information on the ground-state orientation of the anisotropy axis and the distribution of crystal field states within

Received: February 13, 2014
Published: March 20, 2014

   dx.doi.org/10.1021/ja501569t | *J. Am. Chem. Soc.* 2014, 136, 6056−6068

the ground J manifold. Angular-resolved magnetometry studies can provide important experimental validation for such theoretical analysis, though as of yet these have been performed only on a handful of systems.[8c,9] More recently, there have been efforts to develop *a priori* methods for predicting promising f-element single-molecule magnets, based upon electrostatic interactions between the various M_J level electron density distributions and the ligand donor atoms.[7a] For example, a computational method utilizing a pseudopoint charge approximation has been developed to determine the distribution of M_J levels within the ground J manifold of mononuclear lanthanide[10] and actinide[11] complexes, and used further to identify potentially ideal geometries for new systems. More recently, such a point charge approach has been extended to the development of an elegant, simple method for predicting the anisotropy axis orientation in mononuclear lanthanide systems, requiring only atomic coordinates from crystal structure determination, a technique readily accessible to synthetic chemists.[7e]

While it is clear that molecular symmetry is crucial to determining the resultant magnetic properties, no study has yet examined the impact of ligand donor strength within a given coordination geometry. For uranium in particular there is the intriguing possibility of using ligand donor to fine-tune slow magnetic relaxation, given the demonstrated importance of covalency in actinide electronic structure and bonding.[12] Moreover, while covalency is not expected to be a significant factor in lanthanide bonding, it is well-established for lanthanide single-molecule magnets that the electrostatic environment of the ligands strongly predicts magnetic behavior.[7] Thus, altering the ligand environment through the use of soft or hard donors is reasonably expected to influence the magnetic properties.

Most known lanthanide- and actinide-based single-molecule magnets feature hard nitrogen or oxygen donors. Complexes of *N*-donor scorpionate ligands represent the majority of mononuclear U^{3+} single-molecule magnets, which incorporate either bis(pyrazolyl)borate or hydrotris(dimethylpyrazolyl)-borate ligands.[3a,c,e,g,i,13] In addition, Dy^{3+} is known to exhibit slow magnetic relaxation as a homoleptic trischelate complex of the dihydrobis(dimethylpyrazolyl)borate ligand.[13] However, recent efforts have demonstrated the utility of carbon-[3f,k,7b,14] and even sulfur-based donor ligands[5d] in designing new f-element single-molecule magnets. Given the precedent for slow magnetic relaxation in f-element scorpionate complexes and the ready tunability of this ligand platform,[15] we chose to examine donor influence in two new series of isostructural, isomeric complexes $M(Bc^{Me})_3$ ($[Bc^{Me}]^-$ = dihydrobis-(methylimidazolyl)borate) and $M(Bp^{Me})_3$ ($[Bp^{Me}]^-$ = dihydrobis(methylpyrazolyl)borate) for M = Y, Tb, Dy, Ho, Er, and U.

Herein, we show that field-induced slow magnetic relaxation occurs for both complexes incorporating Tb^{3+}, Dy^{3+}, and U^{3+}, though notably the relaxation is orders of magnitude slower for $M(Bc^{Me})_3$, revealing that ligand donor influence is significant for the lanthanides as well as uranium. Additional spectroscopic characterization indicates that this slower relaxation indeed arises from greater magnetocrystalline anisotropy, as engineered through the stronger axial ligand field of the *N*-heterocyclic carbene.

EXPERIMENTAL SECTION

General Considerations. All reactions and subsequent manipulations were performed under anaerobic and anhydrous conditions in a nitrogen-atmosphere glovebox or on a nitrogen-atmosphere Schlenk line. THF, toluene, diethyl ether, and hexanes were dried by passage over activated molecular sieves using a custom-built solvent system. Anhydrous dimethoxyethane (DME) was purchased from Sigma Aldrich and further purified by distillation over sodium benzophenone ketyl, followed by several freeze−pump−thaw cycles to remove dissolved gases. UI_3 was prepared by a modification of the method of Cloke and Hitchcock.[16] Fine uranium powder was synthesized by preparation of UH_3[17] followed by removal of hydrogen under dynamic vacuum at 400 °C. Subsequent heating of the resulting metal powder with a stoichiometric amount of HgI_2 in a sealed tube under vacuum at 320 °C for 2 days afforded the black UI_3 starting material.

Lithium diisopropyl amide (LDA) was prepared by the dropwise addition of one equivalent of 1.6 M *n*-butyllithium to a stirring solution of diisopropyl amine in anhydrous hexanes at −78 °C. Solid white LDA was isolated via canula filtration, and subsequently washed several times with hexanes. Sodium diisopropyl amide (NaDA) was prepared as previously described by combining LDA with sodium *tert*-butoxide in hexanes at room temperature.[18] The compound $K[Bp^{Me}]$ was prepared according to a literature method by heating potassium borohydride with an excess of 2 equiv of 3-methylpyrazole at 120 °C.[19] Crystals of $K[Bp^{Me}]$ used in metathesis reactions to form $M(Bp^{Me})_3$ were isolated through recrystallization from a THF solution layered with hexanes. $Li[Bc^{Me}]$[20] was prepared in a manner similar to that previously described for $Li[Bc^{tBu}]$.[21] THF-d_8 was purchased from Cambridge Isotopes Laboratories and stored over NaK prior to use. Anhydrous $LnCl_3$ was purchased from Strem Chemicals, and diisopropyl amine, 1.6 M solution of *n*-butyllithium in hexanes, 1-methylimidazole, borane dimethylamine, I_2, 3-methylpyrazole, and potassium borohydride were purchased from Sigma Aldrich. Iodine was purified by sublimation, and 3-methylpyrazole was purified by vacuum distillation. All other chemicals were used as received.

NMR spectra were recorded on a Bruker AV 600 spectrometer. IR spectra were recorded on a Perkin-Elmer Avatar Spectrum 400 FTIR spectrometer equipped with ATR. Elemental analyses were performed by the Micro-Mass Facility at the University of California, Berkeley on a Perkin-Elmer 2400 series II combustion analyzer. Quartz tubes used for magnetic samples were custom-made by D&G Glassblowing, Inc.

Li/Na[Bc^{Me}]. Diethyl ether (15 mL) chilled at −34 °C was added to a stirring mixture of $[H_2B(MeIm)_2]I$ and LDA or NaDA (2 equiv) in a reaction vial. After stirring for 3 h, a crystalline white solid deposited in the case of the LDA reaction, while a pale-yellow solution and a beige powder resulted from the NaDA reaction. Attempts to isolate pure $Li[Bc^{Me}]$ through recrystallization were not successful, likely due to the similar solubility of LiI. Rather, what is isolated upon recrystallization is a 1:1 mixture of $Li[Bc^{Me}]$ and LiI, cocrystallized with ∼1 equiv of diethyl ether, as confirmed by elemental analysis. The presence of ∼1 coordinated diethyl ether molecule is also confirmed by ^{1}H NMR of the as-isolated crystalline solid. Clean metathesis reactions resulted when using the solid mixture of LiI and $Li[Bc^{Me}]$ isolated directly by in vacuo removal of diethyl ether solvent and diisopropylamine formed in the reaction. Subsequent removal of Li^+ salts formed in the compound syntheses was achieved by extraction with DME. The absence of additional (organic) impurities beyond the LiI byproduct in the starting $Li[Bc^{Me}]$ material was confirmed by ^{1}H NMR (δ, 400 MHz, THF-d_8): 3.623 (s, 6H, Me); 6.585 (s, 2H, ring); 6.806 (s, 2H, ring). A resonance due to the borate hydrogen atoms was not observed. Calculated for $C_{12}H_{22}BILi2N_4O$ (%) C: 36.96, H: 5.69, N: 14.37; found (%) C: 37.43, H: 5.35, N: 15.66 and (duplicate) C: 36.98, H: 5.56, N: 15.98. This formulation, with one LiI molecule and one coordinated diethyl ether, provided the best match to the obtained elemental analysis.

The Na^+ salt could be readily isolated as highly temperature-sensitive pale-yellow needles by diethyl ether extraction of the beige solid formed in the reaction and storage of the resulting solution at −34 °C (0.175 g, 54% yield). The purity of these crystals was

dx.doi.org/10.1021/ja501569t | J. Am. Chem. Soc. 2014, 136, 6056−6068

confirmed by elemental analysis. Calculated for $C_8H_{12}BN_4Na$ (%) C: 48.52, H: 6.12, N: 28.30; found (%) C: 48.89, H: 5.93, N: 28.19. ^{1}H NMR (δ, 400 MHz, THF-d_8): 3.557 (s, 6H, Me); 6.574 (d, 2H, ring); 6.798 (d, 2H, ring). The Na^+ salt was found to be much more reactive than the Li^+ salt and was not used as a ligand source.

M(Bp^{Me})$_3$ (M = Y, Tb, Dy, Ho, Er, U). At room temperature, a solution of 3 equiv of K[Bp^{Me}] in 6 mL THF was added to a stirring slurry of one equivalent MX_3 in 4 mL THF. The solution rapidly took on the characteristic color of the final corresponding metal complex over the course of ligand addition, and a fine white precipitate formed in solution. After reacting for 3 h, the solution was filtered over 2 cm diatomaceous earth, the solvent removed in vacuo, and the resulting residue redissolved in 10 mL diethyl ether with several drops of THF. The solution was filtered again over Celite, layered with hexanes, and stored at −34 °C. Crystals of M(Bp^{Me})$_3$ would typically form within 1−3 days. Low to moderate yields were obtained from a single crystallization, based on metal halide starting material: 0.135 g (0.692 mmol) of YCl_3 gave 0.170 g of Y(Bp^{Me})$_3$ (40%); 0.0747 g (0.282 mmol) of $TbCl_3$ gave 0.0778 g of Tb(Bp^{Me})$_3$ (40%); 0.0996 g (0.371 mmol) of $DyCl_3$ gave 0.0838 g of Dy(Bp^{Me})$_3$ (46%); 0.132 g (0.485 mmol) of $HoCl_3$ gave 0.025 g of Ho(Bp^{Me})$_3$ (7%); 0.0923 g (0.337 mmol) of $ErCl_3$ gave 0.090o g of Er(Bp^{Me})$_3$ (39%); and 0.150 g (0.242 mmol) of UI_3 gave 0.110 g of U(Bp^{Me})$_3$ (59%). We note that the reported crystalline yield for Ho(Bp^{Me})$_3$ is quite low, and much lower than the other complexes. This value is obtained from a first recrystallization, and is consistently observed, while the crude powder yield(s) appear to be much greater. We ascribe this low yield to greater solubility of this complex in the crystallization solvents used. Calculated for $C_{24}H_{36}B_3N_{12}Y$ (%) C: 46.95, H: 5.91, N: 27.38; found (%) C: 46.96, H: 6.03, N: 27.06. Calculated for $C_{24}H_{36}B_3N_{12}Tb$ (%) C: 42.14, H: 5.31, N: 24.57; found (%) C: 42.09, H: 5.20, N: 24.24. Calculated for $C_{24}H_{36}B_3DyN_{12}$ (%) C: 41.92, H: 5.29, N: 24.45; found (%) C: 41.63, H: 4.99, N: 24.11. Calculated for $C_{24}H_{36}B_3HoN_{12}$ (%) C: 41.78, H: 5.26, N: 24.36; found (%) C: 42.05, H: 5.21, N: 24.15. Calculated for $C_{24}H_{36}B_3ErN_{12}$ (%) C: 41.64, H: 5.24, N: 24.28; found (%) C: 41.49, H: 5.22, N: 24.09. Calculated for $C_{24}H_{36}B_3N_{12}U$ (%) C: 37.78, H: 4.76, N: 22.03; found (%) C: 37.80, H: 4.70, N: 21.80.

M(Bc^{Me})$_3$ (M = Y, Tb, Dy, Ho, Er, U). Separate slurries of one equivalent of MX_3 (M = Y, Tb, Dy, Ho, Er, U; X = I or Cl) in 6 mL THF and ∼3 equiv[22] of LiI·Li[Bc^{Me}] in 6 mL diethyl ether were chilled at −34 °C. With stirring, the metal salt slurry was added dropwise to the slurry of ligand over the course of ∼5 min. Upon complete addition of the metal salt, all reaction components largely dissolved in solution. The mixture was allowed to stir for 3 h, upon which the solution was cloudy with fine solid (Tb, Dy, Y = colorless; Ho, Er = pink; U = dark blue). The supernatant was decanted off of this solid, and 10 mL DME was added to remove LiX. This mixture was stirred for 20 min, and then the solid was isolated and dried under vacuum. Sufficient THF (∼15−20 mL) was added to dissolve the solid, and the resulting solution was filtered over 2 cm diatomaceous earth. Layering of this solution with a 50:50 (v:v) mixture of hexanes and diethyl ether and storage at room temperature resulted in crystals of M(Bc^{Me})$_3$ within 1−3 days. Moderate yields were obtained from a single crystallization, as follows based on metal halide starting material: 0.1113 g (0.5700 mmol) of YCl_3 gave 0.1492 g of Y(Bc^{Me})$_3$ (43%); 0.050 g (0.19 mmol) of $TbCl_3$ gave 0.063 g of Tb(Bc^{Me})$_3$ (48%); 0.050 g (0.19 mmol) of $DyCl_3$ gave 0.076 g of Dy(Bc^{Me})$_3$ (59%); 0.050 g (0.18 mmol) of $HoCl_3$ gave 0.049 g of Ho(Bc^{Me})$_3$ (38%); 0.0462 g (0.169 mmol) of $ErCl_3$ gave 0.0701 g of Er(Bc^{Me})$_3$ (60%); and 0.1135 g (0.1834 mmol) of UI_3 gave 0.05920 g of U(Bc^{Me})$_3$ (42%). Multiple syntheses reproduced crystalline yields between 40 and 60% for each complex. A small amount of additional product could often be obtained from a second recrystallization, although decomposition in solution was evident and likely explains the less than optimum yields of the complexes. Calculated for $C_{24}H_{36}B_3N_{12}Y$ (%) C: 46.95, H: 5.91, N: 27.38; found (%) C: 47.08, H: 5.82, N: 27.45. Calculated for $C_{24}H_{36}B_3N_{12}Tb$ (%) C: 42.14, H: 5.31 N: 24.57; found (%) C: 42.10, H: 5.25, N: 24.38. Calculated for $C_{24}H_{36}B_3DyN_{12}$ (%) C: 41.92, H: 5.29, N: 24.45; found (%) C: 41.64, H: 5.14, N: 24.15. Calculated for $C_{24}H_{36}B_3HoN_{12}$ (%) C: 41.78, H: 5.26, N: 24.36; found (%) C: 41.78, H: 5.31, N: 24.18. Calculated for $C_{24}H_{36}B_3ErN_{12}$ (%) C: 41.64, H: 5.24, N: 24.28; found (%) C: 41.69, H: 5.17, N: 24.11. Calculated for $C_{24}H_{36}B_3N_{12}U$ (%) C: 37.78, H: 4.76, N: 22.03; found (%) C: 38.03, H: 4.96, N: 21.82.

Crystallography. Crystals were mounted on Kapton loops and transferred to a Brüker SMART APEX diffractometer, cooled in a nitrogen stream. The SMART program package was used to determine the unit cell parameters and for data collection (10 s/frame scan time for a hemisphere of diffraction data). Data integration was performed by SAINT and the absorption correction provided by SADABS. Subsequent calculations were carried out using the WinGX program, with structure solutions obtained using SIR2004[23] and subsequent refinements performed using SHELX.[24] The structures were solved by direct methods and refined against F^2 by full-matrix least-squares techniques. The analytical scattering factors for neutral atoms were used throughout the analysis. All nonborate hydrogen atoms were included using a riding model. Electron density corresponding to the borate hydrogen atoms could be found in the Fourier difference map.

Magnetic Measurements. Magnetic samples were prepared by adding crystalline powder compound to a 5 mm inner diameter quartz tube with quartz platform 3/4 of the way down the length of the tube. Solid eicosane was added to cover the samples to prevent crystallite torqueing and provide good thermal contact between the sample and the bath. The tubes were fitted with Teflon sealable adapters, evacuated using a glovebox vacuum pump, and flame-sealed under static vacuum. Following flame sealing, the solid eicosane was melted in a water bath held at 40 °C.

Magnetic susceptibility measurements were collected using a Quantum Design MPMS2 SQUID magnetometer. Dc susceptibility data measurements were performed at temperatures ranging from 1.8 to 300 K, using an applied field of 1000 Oe. The amounts of paramagnetic species present in dilute samples were determined by adjusting the mass of the paramagnetic material until the low-temperature portions of the dilute dc susceptibility curves overlapped with that of the neat compound. Ac magnetic susceptibility measurements were performed using a 4 Oe switching field. All data were corrected for diamagnetic contributions from the core diamagnetism estimated using Pascal's constants[25] to give χ_D = −0.0003378 emu/mol (Y congeners), −0.0003448 emu/mol (Tb/Dy/Ho congeners), −0.0003438 emu/mol (Er congeners), −0.0003718 emu/mol (U congeners), and −0.00024306 emu/mol (eicosane). Cole−Cole plots were fitted using formulas describing χ_M' and χ_M'' in terms of frequency, constant temperature susceptibility (χ_T), adiabatic susceptibility (χ_S), relaxation time (τ), and a variable representing the distribution of relaxation times (α).[26] All data could be fitted to give $\alpha \leq 0.4$ for field-dependent scans, $\alpha \leq 0.32$ for concentrated temperature-dependent scans, and $\alpha \leq 0.25$ for dilute temperature-dependent scans (Tables S3−16 in Supporting Information [SI]).

EPR Measurements. Samples were sealed in quartz tubes with an inner diameter of 4 mm, under Ar, N_2, or static vacuum in the case of solution-phase samples of the Er compounds. EPR spectra were obtained at 2 K with a Varian E-12 spectrometer equipped with flowing liquid He cryostat, an EIP-547 microwave frequency counter, and a Varian E-500 gaussmeter. The data were recorded with a Hewlett-Packard XY plotter, and digitized using the program Un Scan It. The spectra were fit using a version of the code ABVG modified to use the line shape described by Pilbrow and modified to fit spectra using the downhill simplex method.[27,28]

Lanthanide $M_{5,4}$-Edge Measurements. All manipulations were performed with rigorous exclusion of air and moisture using standard Schlenk, glovebox, and glovebag techniques to ensure that trace water or oxygen impurities were removed. Tb_2O_3 was prepared according to the literature method.[29] Samples for STXM measurements were encapsulated between two 100 nm Si_3N_4 membranes (Silson), as described previously.[30] Single-energy images and lanthanide $M_{5,4}$-edge XANES spectra were acquired using the STXM instrument at the Molecular Environmental Science Beamline 11.0.2 at the Advanced Light Source, which is operated in topoff mode at 500 mA, in a < 0.5

dx.doi.org/10.1021/ja501569t | J. Am. Chem. Soc. 2014, 136, 6056−6068

atm He-filled chamber.[31] Energy calibrations were performed at the Ne K-edge for Ne (867.3 eV) or at the Al K-edge for Al foil (1559 eV). The energy resolution (fwhm) was estimated at 0.2 eV, and spectra were collected using elliptically polarized radiation. For these measurements, the X-ray beam was focused with a zone plate onto the sample, and the transmitted X-rays were detected. Images at a single energy were obtained by raster-scanning the sample and collecting X-rays as a function of sample position. Spectra at each image pixel or particular regions of interest on the sample image were extracted from the "stack," which is a collection of images recorded at multiple, closely spaced photon energies across the absorption edge. Dwell times used to acquire an image at a single photon energy were <1 ms per pixel. To quantify the absorbance signal, the measured transmitted intensity (I) was converted to optical density using Beer–Lambert's law: OD = $\ln(I/I_0) = \mu\rho d$, where I_0 is the incident photon flux intensity, d is the sample thickness, and μ and ρ are the mass absorption coefficients and density of the sample material, respectively. Incident beam intensity was measured through the sample-free region of the Si_3N_4 windows. For $Ln(Bp^{Me})_3$ and $Ln(Bc^{Me})_3$, relatively large particles were selected with lateral dimensions $\geq 4\ \mu m^2$. For Ln_2O_3, it was necessary to use smaller particles of area $\leq 0.4\ \mu m^2$ to ensure that they were in the linear regime of the Beer–Lambert law (absorption <1.5 OD). The branching ratio for Tb_2O_3 (0.60) was smaller than expected from the free ion value (0.74),[57a] which may be evidence of small errors due to self-absorption or surface contamination on the small particles. During the STXM experiment, particles showed no sign of radiation damage, and each spectrum was reproduced several times on independent particles and different samples. Second-derivative spectra were used as guides to determine the number and position of peaks, and the areas under the M_5 and M_4 edges were determined graphically by integration of the second-derivative spectra (Figure S50 in SI) using the program *IGOR 6.0*. Branching ratios were reproduced several times from multiple measurements performed on independent samples.

RESULTS AND DISCUSSION

N-heterocyclic carbene ligands are well-known for their strongly σ-donating character and have found utility in stabilizing high-valent transition metal complexes,[32] homogeneous catalysis,[33] and even actinide–lanthanide differentiation.[34] However, *N*-heterocyclic carbene complexes of the f-elements are still fairly sparse, found primarily in heteroleptic systems in which the carbene is tethered to an alkyl chain or stabilized by bulky heteroatom substituents.[35] In one uranyl(VI) β-diketiminate derivative, free methylimidazolate ligands could also be stabilized through "ate" complex formation.[36] No prior examples are present in the literature of Tb^{3+} or Dy^{3+} *N*-heterocyclic carbene complexes, and no homoleptic complexes have been characterized for any f-element. Previous metal complexes of the ligand $[Bc^{Me}]^-$ were limited to gold, palladium, and platinum, and in these cases the ligand was not isolated or characterized spectroscopically, but prepared *in situ* by deprotonation of $[H_2B(MeIm)_2]I$ with *n*-butyllithium.[20] Thus, the $M(Bc^{Me})_3$ complexes reported here represent the first examples of *N*-heterocyclic carbene complexes of terbium and dysprosium, and also the first examples of homoleptic *N*-heterocyclic carbene complexes for any f-element.

Our synthetic approach to $Li[Bc^{Me}]$ closely followed the route established by Nieto and co-workers for the synthesis of $Li[Bc^{tBu}]$.[21] Interestingly, the precursor imidazolium salt $[H_2B(MeIm)_2]I$ is an ionic liquid above 100 °C. The compounds $Li[Bc^{Me}]$ and $Na[Bc^{Me}]$ were prepared via deprotonation of $[H_2B(MeIm)_2]I$ with 2 equiv of the corresponding diisopropyl amide in diethyl ether at −34 °C. Both salts could be isolated as highly temperature-sensitive crystalline solids, free of organic impurities as indicated by ^1H NMR spectroscopy; however, it was not possible in our hands to isolate LiI-free crystals of $Li[Bc^{Me}]$, as indicated by elemental analysis. In contrast, $Na[Bc^{Me}]$ could be recrystallized from diethyl ether as pale yellow needles and proved to be pure by elemental analysis. Due to the greater temperature sensitivity and reactivity of $Na[Bc^{Me}]$, however, only $Li[Bc^{Me}]$ was used in the synthesis of $M(Bc^{Me})_3$.

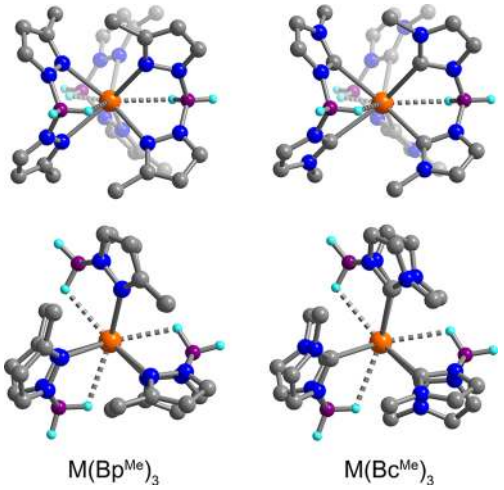

Figure 1. Side and top views of X-ray crystal structures of the trigonal prismatic complexes $M(Bp^{Me})_3$ and $M(Bc^{Me})_3$ for M = U. The lanthanide congeners are isostructural. Orange, gray, blue, purple, and pale-blue spheres representing U, C, N, B, and H atoms, respectively; all other hydrogen atoms have been omitted for clarity. The borate hydrogen atoms were found in the Fourier difference map, confirming agostic M···H–BH interactions.

Initial attempts to synthesize $M(Bc^{Me})_3$ in THF at room temperature led to a mixture of products, of which the desired complex was frequently a minor component. Cooling the reaction to −34 °C also did not increase the yield significantly. Instead, it was found that using a mixture of diethyl ether and THF (50% diethyl ether or more by volume) led to highly reproducible syntheses of $M(Bc^{Me})_3$ in moderate yields. Accordingly, a slurry of metal salt in THF was chilled to −34 °C and added dropwise to a stirring slurry of LiI·$Li[Bc^{Me}]$ in diethyl ether, also at −34 °C. After stirring for 3 h, solid $M(Bc^{Me})_3$ had precipitated from the reaction mixture and could be readily isolated by decanting off the supernatant and stirring the resulting solid in DME to remove excess LiI or LiCl.

Crystals of $M(Bc^{Me})_3$ grow in the course of 1–3 days at room temperature, from a THF solution layered with a 50:50 (v:v) mixture of hexanes and diethyl ether. The crystals form as beautiful rectangular blocks with considerable luster, and are deep royal blue for U^{3+}, colorless for Tb^{3+}, Dy^{3+}, and Y^{3+}, and neon and pale pink for Ho^{3+} and Er^{3+}, respectively. When crystalline, these compounds are only minimally soluble in THF and completely insoluble in other ethereal or aromatic solvents. The compounds $M(Bc^{Me})_3$ are air- and temperature-sensitive and start to decompose within a few days under nitrogen when left in the solid state at room temperature. Interestingly, $Ho(Bc^{Me})_3$ appears bright pink under illumination with a mercury vapor lamp, while under broad spectrum light it is pale yellow (Figure S1 in SI), a common phenomenon for Ho^{3+} compounds arising from sharp phosphor-like emission.[37]

The compounds $M(Bp^{Me})_3$ were synthesized at room temperature from the combination of the corresponding

dx.doi.org/10.1021/ja501569t | J. Am. Chem. Soc. 2014, 136, 6056–6068

Table 1. Selected Bond Lengths (Å) and Angles (deg)

cmpd	M−N or C[a]	bite angle	intercentroid[b]	M···H	M···B	M···M	normalized bite
$U(Bp^{Me})_3$	2.588(4)	76.73(9)	3.2105(3)	2.62(4)	3.201(5)	9.427(1)	1.241(2)
$U(Bc^{Me})_3$	2.662(4)	73.77(9)	3.188(2)	2.75(2)	3.334(4)	8.482(5)	1.200(2)
$Tb(Bp^{Me})_3$	2.491(3)	78.99(5)	3.1680(1)	2.44(2)	3.113(3)	9.508(1)	1.272(2)
$Tb(Bc^{Me})_3$	2.578(3)	75.55(5)	3.1533(2)	2.74(2)	3.282(2)	8.699(1)	1.225(2)
$Dy(Bp^{Me})_3$	2.481(3)	78.94(5)	3.1535(2)	2.48(2)	3.103(3)	9.496(1)	1.271(2)
$Dy(Bc^{Me})_3$	2.577(4)	75.40(9)	3.148(2)	2.75(3)	3.277(4)	8.919(1)	1.223(2)
$Ho(Bp^{Me})_3$	2.473(3)	79.12(6)	3.2921(2)	2.43(2)	3.091(3)	9.491(1)	1.277(2)
$Ho(Bc^{Me})_3$	2.556(3)	75.49(6)	3.1246(1)	2.71(2)	3.273(3)	8.743(1)	1.224(2)
$Er(Bp^{Me})_3$	2.463(3)	79.11(6)	3.1360(3)	2.42(2)	3.086(2)	9.482(1)	1.274(2)
$Er(Bc^{Me})_3$	2.545(3)	75.56(5)	3.1183(2)	2.71(2)	3.271(2)	8.771(1)	1.225(2)
$Y(Bp^{Me})_3$	2.474(1)	78.95(5)	3.1440(2)	2.41(1)	3.100(3)	9.483(3)	1.271(1)
$Y(Bc^{Me})_3$	2.565(2)	75.39(5)	3.1314(2)	2.71(2)	3.280(3)	8.731(1)	1.223(1)

[a]Averages of the two crystallographically independent values. [b]Distance between two centroids defined by upper and lower planes of coordinated carbon (nitrogen) atoms.

metal halide and potassium salt of the ligand in THF. This reaction proceeds cleanly at room temperature and is not significantly dependent on the identity of the reaction solvent or manner of combination of metal salt and ligand. Further in contrast to $M(Bc^{Me})_3$, the $M(Bp^{Me})_3$ complexes readily crystallize at low temperature and are highly soluble in THF, with good solubility in DME or 2-MeTHF, and limited solubility in diethyl ether. These species can also be stored indefinitely under nitrogen at room temperature without decomposition. Crystals of the $M(Bp^{Me})_3$ complexes grow within 1−3 days at −34 °C from a mixture of diethyl ether and THF or 2-MeTHF layered with hexanes. The crystals also form as rectangular blocks, and are dark burgundy in the case of U^{3+}, colorless for Tb^{3+}, Dy^{3+}, and Y^{3+}, and neon and pale pink for Ho^{3+} and Er^{3+}, respectively; crystals of $Ho(Bp^{Me})_3$ exhibit the same color change as $Ho(Bc^{Me})_3$.

Both $M(Bp^{Me})_3$ and $M(Bc^{Me})_3$ complexes crystallize in the space group $R\bar{3}$, with idealized C_{3h} symmetry (see Figure 1), where the presence of agostic M···H−BH interactions leads to an overall tricapped trigonal prismatic coordination geometry. Such agostic interactions are observed for metal complexes of scorpionate ligands,[38] and can be identified as a manifold of infrared stretches in the range of 2200−2500 cm^{-1} (Figure S3 in SI). Electron density corresponding to $-BH_2$ protons could be found in the Fourier difference map of all complexes, and the resulting M···H−BH interaction distances along with metal−donor distances are given in Table 1.

The M−N[13,38cd] or M−C[34,35] bond lengths for each complex are in agreement with previously reported values, with the M−C distances consistently longer than the M−N distances by as much as 0.1 Å. Notably, the M−N separations in the $M(Bp^{Me})_3$ complexes are the same within error when the ionic radius of the lanthanide ion is excluded, and the same is true for the M−C distances in $M(Bc^{Me})_3$; thus, these metrical parameters alone would suggest that the bonding is best described as ionic for both types of complexes.[39] Additional structural features of note are the ligand bite angles, agostic M···H distances, and nearest neighbor M···M distances. The ligand bite angles for the $M(Bc^{Me})_3$ complexes are smaller by more than 3° when compared to the corresponding $M(Bp^{Me})_3$ complexes, and these are accompanied by agostic M···H interaction distances that are larger on average by ∼0.3 Å. Values of the normalized bite angles calculated for all complexes by the method of Kepert (Table 1)[40] reveal that these differences are statistically significant, with a smaller normalized bite associated with the

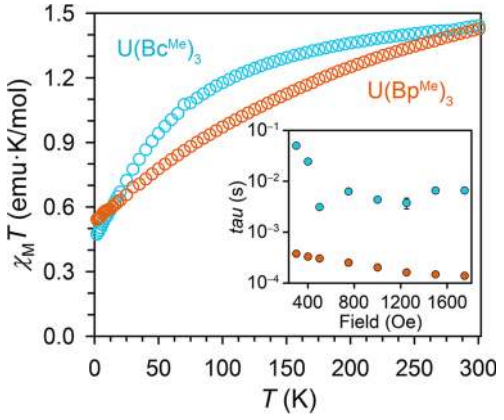

Figure 2. Plot of the molar magnetic susceptibility times temperature vs temperature ($\chi_M T$ vs T) for $U(Bc^{Me})_3$ (blue circles) and $U(Bp^{Me})_3$ (orange circles) collected under an applied field of 0.1 T. For free U^{3+} $\chi_M T$ = 1.63 emu·K/mol (L−S coupling). (Inset) Plot of the relaxation time vs H_{dc} for $U(Bc^{Me})_3$ and $U(Bp^{Me})_3$ at 1.8 K.

$M(Bc^{Me})_3$ complexes. Furthermore, the distance between centroids defined by the upper and lower nitrogen (carbon) atoms is smaller for $M(Bc^{Me})_3$. Thus, coordination of the *N*-heterocyclic carbene ligands leads to formation of a trigonal prism that is more axially compressed than that formed by coordination of the bis(pyrazolyl)borate ligands. From a purely electrostatic argument, we might therefore expect that the crystal field in $M(Bc^{Me})_3$ will be more favorable in promoting slow relaxation for oblate f-element ions.

Static Magnetic Susceptibility. Magnetic susceptibility data were collected for the $M(Bp^{Me})_3$ and $M(Bc^{Me})_3$ compounds under a static field of 1000 Oe (Figures 2 and S6 in SI). In the case of U^{3+}, these measurements provide information about the splitting of the $J = {}^9/_2$ ground state manifold by the crystal field, which removes the degeneracy of the corresponding M_J states. In C_{3h} symmetry, the $^4I_{9/2}$ ground state forms five Kramers doublets: the $M_J = \pm {}^1/_2$ doublet, two doublets that are mixtures of $M_J = \pm {}^9/_2$ and $\mp {}^3/_2$, and two that are mixtures of $M_J = \pm {}^7/_2$ and $\mp {}^5/_2$.

As the temperature is raised from zero K, $\chi_M T$ increases due to two factors. At the lowest temperatures, only the ground state is populated, and the slope is typically due to temperature-independent paramagnetism, the value of which is inversely proportional to the energy gap between the two lowest M_J doublets.[41] In this regime, $\chi_M T$ is linear with temperature, as in

dx.doi.org/10.1021/ja501569t | J. Am. Chem. Soc. 2014, 136, 6056−6068

Table 2. Parameters Obtained from Fitting Temperature-Dependent Ac Susceptibility for $M(Bp^{Me})_3$ and $M(Bc^{Me})_3$

cmpd	U_{eff}[a] (cm^{-1})	τ_0 (s)	A ($s^{-1} \cdot K^{-1}$)	A ($s^{-1} \cdot K^{-2}$)	C ($s^{-1} \cdot K^{-5}$)	C ($s^{-1} \cdot K^{-7}$)	C ($s^{-1} \cdot K^{-9}$)
$U(Bp^{Me})_3$	–	–	1271(3)	–	23.09(4)	–	–
11% $U(Bp^{Me})_3$	–	–	262(3)	–	9.69(2)	–	–
$U(Bc^{Me})_3$	31.668(1)	1×10^{-7}	77.317(6)	–	1.1294(2)	–	–
12% $U(Bc^{Me})_3$	33.328(3)	1×10^{-7}	0	–	0.1863(4)	–	–
14% $Tb(Bp^{Me})_3$	21(1)	$1(1) \times 10^{-6}$	115.9(7)	–	–	0.0013(1)	–
$Tb(Bc^{Me})_3$	44.8(2)	$8.6(2) \times 10^{-6}$	–	0.527(4)	–	–	–
11% $Tb(Bc^{Me})_3$	45.2(4)	$6.6(4) \times 10^{-6}$	–	0.23(1)	–	–	–
$Dy(Bc^{Me})_3$	32.8(7)	$6(1) \times 10^{-9}$	3.1(3)	–	–	–	–
12% $Dy(Bc^{Me})_3$	33.6(3)	$4.2(4) \times 10^{-9}$	0.39(9)	–	–	–	0.00057(8)

[a]Data acquired under H_{dc} = 1500 Oe except in the case of concentrated $U(Bc^{Me})_3$ (H_{dc} = 750 Oe) and $U(Bp^{Me})_3$ (H_{dc} = 300 Oe).

the $U(Bc^{Me})_3$ data between zero and 50 K. As the temperature increases, other low-lying states become thermally populated. For these states, the magnitude of the temperature-independent paramagnetism is the same, but it is of opposite sign to that of the ground state, and the slope of $\chi_M T$ vs T will thus decrease, as seen at ~70 K for $U(Bc^{Me})_3$.[41]

As the temperature is increased and $k_B T$ becomes significantly greater than the splitting within the $J = {}^9/_2$ manifold, the Kramers doublets are equivalently populated, and $\chi_M T$ becomes largely temperature independent, approaching the free-ion value.[42] For both $U(Bp^{Me})_3$ and $U(Bc^{Me})_3$, the room temperature $\chi_M T$ values of 1.43 and 1.44 emu·K/mol, respectively, are significantly lower than the value of 1.63 emu·K/mol calculated for a free f^3 ion, although still within range of previously reported values for U^{3+} complexes.[3,13] This low room temperature value of $\chi_M T$ may arise from two possibilities. First, if the crystal field splitting is large relative to $k_B T$ at 300 K, the population of the Kramers doublets in the $J = {}^9/_2$ manifold will not be complete, and the plot of $\chi_M T$ vs T will have a significant slope, as is the case for $U(Bp^{Me})_3$. This suggests that $U(Bp^{Me})_3$ possesses a larger crystal field splitting than $U(Bc^{Me})_3$.

The presence of significant covalency in the bonding between ligands and the U^{3+} center can also lead to a $\chi_M T$ value much less than that of the free-ion value,[43] as the orbital angular momentum of the occupied f-orbitals is reduced. While the value of $\chi_M T$ for $U(Bc^{Me})_3$ is only slightly temperature dependent at 300 K, consistent with a small crystal field splitting relative to room temperature, that of $U(Bp^{Me})_3$ is still strongly temperature dependent. This suggests that the magnitude of $\chi_M T$ will be greater for $U(Bp^{Me})_3$ when the $J = {}^9/_2$ multiplet is fully populated, and therefore that the bonding in $U(Bc^{Me})_3$ is more covalent.

For M = Tb^{3+}, Dy^{3+}, Ho^{3+}, and Er^{3+}, the room temperature $\chi_M T$ values are 11.74 and 12.14 emu·K/mol, 14.05 and 13.90 emu·K/mol, 14.16 and 13.78 emu·K/mol, and 11.62 and 11.58 emu·K/mol for the $M(Bp^{Me})_3$ and $M(Bc^{Me})_3$ complexes, respectively, agreeing well with those anticipated for the free ions (11.82, 14.17, 14.07, and 11.48 emu·K/mol).[44] For each metal, the temperature dependence of $\chi_M T$ is similar between isomers (Figure S6 in SI) in contrast to the uranium congeners. The similarity of the room temperature moments of $Ln(Bp^{Me})_3$ and $Ln(Bc^{Me})_3$ to the free ion values strongly suggests that covalency is small (compared to $k_B T$ at room temperature) in both sets of compounds. Likewise, the low temperatures at which the $\chi_M T$ vs T plots flatten out strongly suggest that the crystal field splitting is weak for all of the complexes, with the possible exception of the Tb^{3+} species.

Variable-Field Ac Magnetic Susceptibility. A hallmark of single-molecule magnetism is slow magnetic relaxation in the presence of a small oscillating magnetic field, leading to the presence of an out-of-phase component, χ_M'', to the magnetic susceptibility. In the presence of a 4 Oe oscillating field and zero external field over the frequency range of 1−1500 Hz, no full χ_M'' peak was observed for $M(Bp^{Me})_3$ or $M(Bc^{Me})_3$. However, many factors can lead to the absence of slow magnetic relaxation under zero applied field, including the presence of dipolar interactions and zero-field tunneling,[45] the latter having particular relevance for non-Kramers ions (i.e., ions with an even number of electrons) such as Tb^{3+} and Ho^{3+}. In such cases, application of a dc field can suppress tunneling or break up transverse fields caused by dipolar interactions, and reveal slow magnetic relaxation.[45] Indeed, at 1.8 K under a small applied dc field of less than 500 Oe, an out-of-phase signal becomes apparent for the complexes $M(Bp^{Me})_3$ and $M(Bc^{Me})_3$ (M = Tb^{3+}, Dy^{3+}, and U^{3+}) (Figures S7−S14 in SI). For the $M(Bc^{Me})_3$ species, the relaxation is generally characterized by high-frequency χ_M'' peaks under small applied dc fields, which grow in magnitude and move to lower frequencies as the field is increased. In the cases of Tb and $Dy(Bp^{Me})_3$, only high-frequency tails are observed in χ_M'' for fields as high as 1250 Oe, precluding further analysis of the relaxation behavior in the concentrated samples.[46] However, for all compounds, the relaxation time is notably 1−2 orders of magnitude slower for $M(Bc^{Me})_3$ than for the corresponding $M(Bp^{Me})_3$ complex (Figures 2, inset, and S7−S14 in SI). Note that the optimum applied magnetic field used below in temperature-dependent measurements corresponds to a simultaneous maximum in χ_M'' and τ.

Variable-Temperature Ac Magnetic Susceptibility. The compounds $M(Bc^{Me})_3$ (M = Tb, Dy, U) and $U(Bp^{Me})_3$ all demonstrate temperature-dependence in χ_M''. However, the corresponding plots of $\ln(\tau)$ vs $1/T$ show pronounced deviations from linearity (Figures S23−26 in SI), indicating that thermally activated Orbach relaxation is not the dominant spin−lattice relaxation process. In such a scenario, commonly only the highest temperature points are fit to extract a value of the relaxation barrier, U_{eff}. However, this method provides only an estimate of U_{eff}, making a comprehensive comparison of relaxation behavior challenging. By considering the other possible spin−lattice relaxation mechanisms, namely Raman[47] and direct[48] processes, it is possible to fit the entire range of temperature-dependent relaxation.[49,50] This was accomplished by employing eq 1[51] and enabled determination of the contribution from each spin−lattice mechanism in $M(Bp^{Me})_3$ and $M(Bc^{Me})_3$. In this equation, the first, second, and third terms account for the temperature-dependence of direct,

dx.doi.org/10.1021/ja501569t | J. Am. Chem. Soc. 2014, 136, 6056−6068

Orbach, and two-phonon Raman relaxation processes, respectively. Orbach and Raman processes can both be observed under zero dc field, while in the presence of applied fields the possibility of direct relaxation between out-of-resonance ground states becomes highly relevant. The exponents n and m have been shown to take on various values with the direct process commonly showing linear or quadratic dependence on temperature (n = 1 or 2), while the exponent of the Raman process is highly dependent on the identity of the metal ion and the energy separations between lowest-lying Kramers doublets (see refs 50b and 52). The parameters obtained from fitting are summarized in Table 2.

$$\tau^{-1} = AT^{n} + \tau_0^{-1} \exp(-U_{\text{eff}}/k_B T) + CT^{m} \quad (1)$$

Uranium. Under an applied field of 750 Oe, a χ_M'' signal is observed from 1.7 to 4.1 K for $U(Bc^{Me})_3$ (Figure S15 in SI). Relaxation times were extracted for this range of temperatures by fitting Cole−Cole plots using a generalized Debye model.[26] Fitting the corresponding plot of $\ln(\tau)$ vs $1/T$ to eq 1 reveals that Orbach relaxation dominates at high temperatures, with U_{eff} = ~32 cm^{-1}. A very small contribution from a Raman process is also evident, while direct relaxation occurs at low temperatures (Table 2 and Figure S23 in SI). In contrast, $U(Bp^{Me})_3$ demonstrates a much weaker temperature dependence under a 300 Oe applied field (Figure S16 in SI), and a plot of $\ln(\tau)$ vs $1/T$ can be fit with only direct and Raman contributions (Table 2 and Figure S24 in SI).[52]

Terbium. The slowest relaxation among all of the compounds occurs for $Tb(Bc^{Me})_3$, for which an applied field of 1500 Oe leads to the presence of a χ_M'' signal from 4 to 19 K within the measured frequency range (Figure S18 in SI). $Tb(Bc^{Me})_3$ also exhibits the largest relaxation barrier at U_{eff} = 44.8(2) cm^{-1} (Table 2 and Figure S25 in SI).

Dysprosium. Under a 1500 Oe applied field, $Dy(Bc^{Me})_3$ relaxes slowly over the temperature range 2.5 to 4.6 K. Values of the α parameter at this field indicate a narrow distribution of relaxation times ($\alpha \leq 0.2$),[26] although a clearly resolved second process grows in at low frequencies, accounting for a very small magnitude of the total susceptibility (Figure S21 in SI).[53] Fitting of the temperature-dependence of the dominant process reveals that the relaxation is thermally activated, with U_{eff} = 32.8(7) cm^{-1} and $\tau_0 = 6(1) \times 10^{-9}$ s (Table 2 and Figure S26 in SI).

Dilution Studies. To further aid in the comparison of relaxation behavior, ac magnetic susceptibility measurements were performed on crystalline dilute samples prepared with $Y(Bc^{Me})_3$ and $Y(Bp^{Me})_3$ compounds. These measurements confirm the molecular origins of the observed slow magnetic relaxation, and provide even stronger evidence of the advantage of the *N*-heterocyclic carbene ligand. At 1.8 K the relaxation time for 12 mol % $U(Bc^{Me})_3$ is orders of magnitude slower than in the concentrated species, and field-dependent frequency scans at 3.5 K reveal only a single peak, indicating uniform relaxation (Figure S27 in SI). Fitting of the temperature-dependent relaxation data collected at 1500 Oe reveals predominantly Orbach relaxation with $U_{\text{eff}} \approx$ 33 cm^{-1}, and the direct process is no longer operative (Figure 3, Table 2, and Figure S31 in SI). For a sample of 11 mol % $U(Bp^{Me})_3$ in $Y(Bp^{Me})_3$, the relaxation time is slowed only by a factor of 4, and the direct process remains dominant (Figures S32−36 in SI).

For 11 mol % $Tb(Bc^{Me})_3$ cocrystallized with $Y(Bc^{Me})_3$, slow relaxation is present under zero applied dc field as a tail at the highest frequencies. Under an applied field of 1500 Oe, the temperature range of observable χ_M'' signal extends from 5.2 to 19.2 K (Figure 3), and the relaxation time has increased below 8 K compared to the concentrated sample. Moreover, the contribution of the direct process is now half of what it was in the concentrated sample, and the relaxation barrier has increased to U_{eff} = 45.1(4) cm^{-1} (Table 2).

Dilution of $Tb(Bp^{Me})_3$ results in an observable χ_M'' signal from 1.7 to 7.45 K under an applied field of 1500 Oe (Figure S41 in SI), although the relaxation occurs largely via direct and Raman processes. A small contribution from Orbach relaxation is fit at the highest temperatures (Figure S43 in SI), yet still the estimated barrier is less than half of that for $Tb(Bc^{Me})_3$ (Table 2).

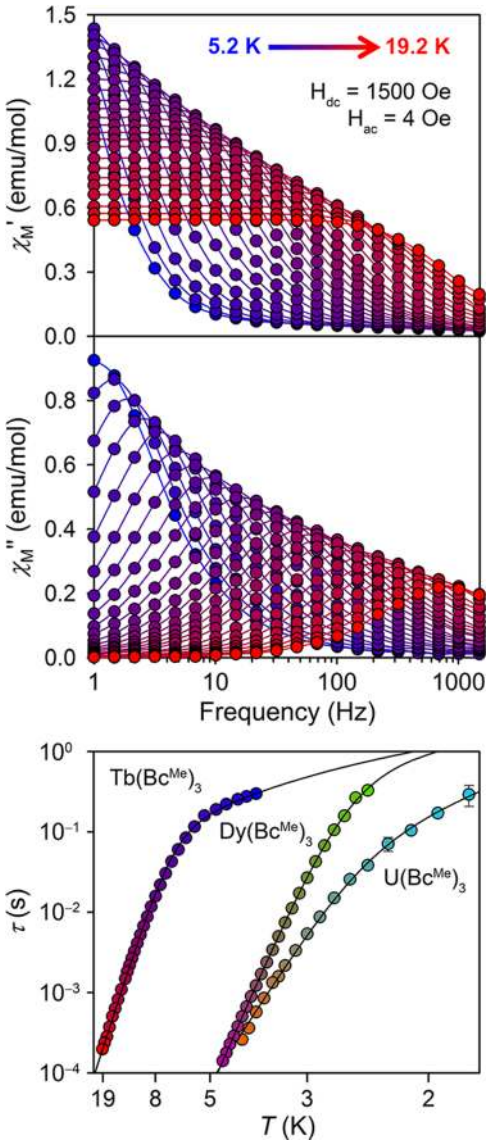

Figure 3. (Upper) Plot of the in-phase (χ_M') and out-of-phase (χ_M'') magnetic susceptibility for 11 mol % $Tb(Bc^{Me})_3$ under an applied field of 1500 Oe. (Lower) Plot of the relaxation time τ (log scale) vs T (inverse scale) for samples of 11% Tb, 12% Dy, and 12% $U(Bc^{Me})_3$ under H_{dc} = 1500 Oe. Percentages represent molar quantities of the paramagnetic complex present in a matrix of $Y(Bc^{Me})_3$. Fitting to eq 1 yields U_{eff} = 45.2(4) cm^{-1} ($Tb(Bc^{Me})_3$), 33.6(3) cm^{-1} ($Dy(Bc^{Me})_3$), and ~33 cm^{-1} ($U(Bc^{Me})_3$), with $\tau_0 = 6.6(4) \times 10^{-6}$ s, $4.2(4) \times 10^{-9}$ s, and 1×10^{-7} s, respectively.

dx.doi.org/10.1021/ja501569t | J. Am. Chem. Soc. 2014, 136, 6056−6068

A sample of 11 mol % $Dy(Bp^{Me})_3$ in $Y(Bp^{Me})_3$ displays only very broad and featureless peaks under applied fields, precluding any analysis of relaxation behavior. However, for a 12 mol % sample of $Dy(Bc^{Me})_3$ in $Y(Bc^{Me})_3$ the relaxation time slows greatly, and χ_M'' signal can be seen even under zero dc field, although only at the highest measured frequencies, as observed for $Tb(Bc^{Me})_3$. This peak is very broad, suggesting multiple relaxation processes; however, application of a 1500 Oe field results in uniform peaks from 2.4 to 4.6 K (Figure S46 in SI). For this sample, the coefficient for the direct process decreases by nearly an order of magnitude (Table 2), and the relaxation is clearly dominated by an Orbach process (Figures 3 and S48 in SI). From this data, U_{eff} = 33.6(3) cm^{-1} and τ_0 = 4.2(4) × 10^{-9} s are calculated, in good agreement with the concentrated sample.

The relaxation parameters determined from fitting the data for each complex are summarized in Table 2. Taking the values obtained from the dilute samples, which more accurately represent the intrinsic single-molecule relaxation, the experimental values of U_{eff} are small, although within range of those previously reported for mononuclear systems.[2] In the case of $U(Bc^{Me})_3$, the relaxation barrier of ∼33 cm^{-1} is the highest yet reported for a mononuclear uranium species. The observation of slow magnetic relaxation only for the Tb^{3+}, Dy^{3+}, and U^{3+} compounds supports the underlying principle that an axial ligand field favors the development of a relaxation barrier for oblate f-element ions.[54] However, the relaxation is significantly slower for the corresponding $M(Bc^{Me})_3$ compounds and is dominated by an Orbach process, despite closer interion distances compared to those for $M(Bp^{Me})_3$. Clearly, the presence of a carbon donor in the $M(Bc^{Me})_3$ complexes serves to lengthen τ and facilitates relaxation through thermal means. Considering again a crystal field model, it could be argued that the much slower relaxation for $M(Bc^{Me})_3$ results in part from the axial compression of this crystal field relative to $M(Bp^{Me})_3$ (*vida supra*). In order to further probe electronic differences in these two complexes, we turned to $M_{5,4}$-edge, EPR, and ^1H NMR spectroscopies.

Lanthanide XANES. Of the experimental approaches to evaluate electronic structure in lanthanide materials, XANES has historically formed an important component of the characterization of complex systems with many-electron or open-shell configurations.[55] Exciting electrons from 3d core orbitals at the M_5 and M_4 edges is a particularly effective method because it probes the valence 4f orbitals directly with electric dipole-allowed transitions of $\Delta l \pm 1$.[56] For the free ion, these $M_{5,4}$-edge transitions can be described as $3d^{10}4f^n \rightarrow 3d^9 4f^{n+1}$ excitations, which are split into two primary M_5 ($3d_{5/2} \rightarrow 4f_{7/2}$ and $3d_{5/2} \rightarrow 4f_{5/2}$) and M_4 ($3d_{3/2} \rightarrow 4f_{5/2}$) edges due to differences in the stabilization of the spin−orbit split $3d_{5/2}$ and $3d_{3/2}$ core holes (Figure 4, left).[57] Previous studies have shown that the ratio of intensities for the lower-energy M_5 and higher-energy M_4 edges are sensitive to changes in the local chemical environment dictated by spin−orbit and covalency effects.[58]

Chemical bonding and electronic structures were evaluated for $Ln(Bp^{Me})_3$ and $Ln(Bc^{Me})_3$ by determining the branching ratios from $M_{5,4}$-edge XANES. This approach has been successful in detailed studies of lanthanide oxides,[58a,59] metals,[57a] and various other lanthanide-containing materials.[60] The sesquioxides Ln_2O_3 (Ln = Tb, Dy, Ho, Er) were measured as a reference, given that the lanthanide ions in this environment are well-described by a rigorously trivalent electronic configuration.[58a,61] Accurate measurements were facilitated by using a scanning transmission X-ray microscope (STXM).

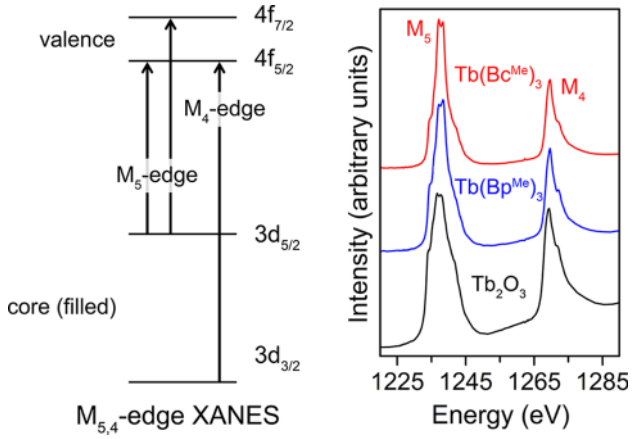

Figure 4. (Left) Qualitative energy level diagram showing allowed electronic transitions at the $M_{5,4}$ edges. Spin−orbit coupling with the core hole splits the $3d_{3/2}$ and $3d_{5/2}$ orbitals by ∼20−40 eV (for Tb through Er). To a lesser extent, spin−orbit coupling, ligand-field, and multiplet effects cause scrambling of the valence $4f_{5/2}$ and $4f_{7/2}$ levels. (Right) Background-subtracted terbium $M_{5,4}$-edge XANES spectra from $Tb(Bc^{Me})_3$, $Tb(Bp^{Me})_3$, and Tb_2O_3.

Figure 4 shows the background subtracted $M_{5,4}$-edge spectra for $Tb(Bc^{Me})_3$, $Tb(Bp^{Me})_3$, and Tb_2O_3 (see Figure S49 in SI for Ln = Dy, Ho, Er) obtained using STXM. For each of the compounds, the strong spin−orbit interaction in the core hole separates the M_5 and M_4 edges into two distinct regions, with separations of approximately 32 eV for Tb and 42 eV for Er. At first glance, each of the spectral profiles is similar to those expected on the basis of predictions for the free ions,[58a] with M_5 and M_4 edges exhibiting many multiplet features. The low-energy M_5 edges exhibit considerable structure and a characteristic sawtooth pattern, followed by a tail that decreases mostly to zero. However, the well-defined sharp features on the M_5 edge belie an extremely complex underlying spectrum consisting of hundreds or even thousands of unique transitions.[57a,58a] At high energy, the M_4 edge does not exhibit the same quantity of multiplet features, but it is clearly asymmetric in appearance and likely composed of multiple transitions.

The branching ratios $A_5/(A_5 + A_4)$, where A_5 and A_4 are the areas under the M_5 and M_4 peaks, were determined using a graphical approach based on integration of the second derivative spectrum (Figure S50 in SI).[58b] The branching ratios determined for $Ln(Bc^{Me})_3$, $Ln(Bp^{Me})_3$, and Ln_2O_3 (Ln = Tb, Dy, Ho, Er) are listed in Table S17 in SI and plotted in Figure 5 as a function of the number of 4f electrons in the initial state. For all three sets of compounds, larger branching ratios are observed with increases in atomic number and the concomitant increase in the number of 4f electrons in the initial state. This trend is consistent with previous studies,[57a,58a,59,60] which have shown that the branching ratio approaches unity as the lanthanide series is traversed from left to right because the $4f_{5/2}$ states are filled first and the probability of the $3d_{3/2} \rightarrow 4f_{5/2}$ (M_4) excitation decreases. This phenomenon is exemplified by the case of Yb^{3+} ($4f^{13}$), in which the $4f_{5/2}$ states are filled completely and only the $3d_{5/2} \rightarrow 4f_{7/2}$ (M_5) excitation is allowed.[57a]

Although the three sets of compounds exhibit the anticipated trend toward increasing branching ratios, values for individual

dx.doi.org/10.1021/ja501569t | J. Am. Chem. Soc. 2014, 136, 6056−6068

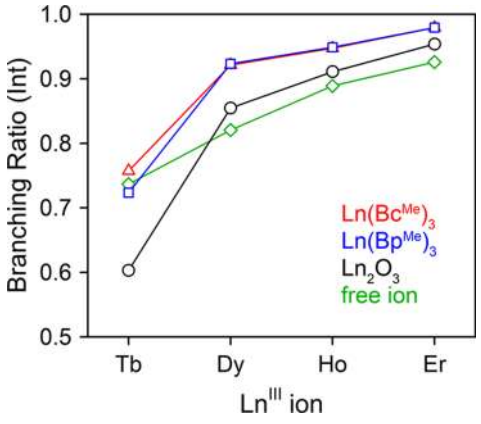

Figure 5. Plot of the branching ratios determined from the experimental $M_{5,4}$-edge XANES spectra of $Ln(Bc^{Me})_3$, $Ln(Bp^{Me})_3$, and Ln_2O_3 for Ln = Tb, Dy, Ho, and Er. The experimentally determined branching ratio for Tb_2O_3 (0.60) is smaller than expected on the basis of theoretical free ion values (see Experimental Section). Theoretical free ion values are taken from reference 57a.

lanthanides were uniformly higher for $Ln(Bp^{Me})_3$ and $Ln(Bc^{Me})_3$ relative to the corresponding oxides (Figure 5). For example, values determined for both $Tb(Bp^{Me})_3$ (0.76) and $Tb(Bc^{Me})_3$ (0.72) were significantly higher than those for Tb_2O_3 (0.60). Toward the end of the series, the branching ratio measured for Er_2O_3 (0.95) was lower than that of either $Er(Bp^{Me})_3$ or $Er(Bc^{Me})_3$ (both 0.98). Although changes in the crystal field are unlikely to be reflected in branching ratios,[57b] trends toward increasing branching ratios may be rationalized by enhanced covalent mixing with high-energy donor orbitals on the $[Bp^{Me}]^-$ and $[Bc^{Me}]^-$ ligands. Electrons will preferentially occupy the $4f_{5/2}$ levels, which decreases the probability of the $3d_{3/2} \rightarrow 4f_{5/2}$ (M_4) transitions and increases the branching ratios in $Ln(Bp^{Me})_3$ and $Ln(Bc^{Me})_3$ relative to Ln_2O_3.[57a,58,62] Although electronic structure calculations and additional spectroscopic measurements are needed to fully validate this interpretation, the $M_{5,4}$-edge XANES results suggest that the $[Bp^{Me}]^-$ and $[Bc^{Me}]^-$ ligands both provide a more strongly donating ligand field in comparison with the trivalent Ln_2O_3.

EPR Spectroscopy and Metal Ion Anisotropy. EPR can be a powerful experimental probe to understand low-temperature slow magnetic relaxation in single-molecule magnets, allowing for assessment of magnetic anisotropy through determination of the electronic *g*-values and the magnetic ground state.[63] Low-temperature X-band EPR spectra were collected for compounds of the Kramers ions Dy^{3+}, Er^{3+}, and U^{3+}. Data collected at 2 K reveal anisotropic signals for Er^{3+} (Figure S51−53 in SI) and U^{3+} (Figure 6), each with dominant transverse anisotropy ($g_\perp > g_\parallel$). Both $Dy(Bp^{Me})_3$ and $Dy(Bc^{Me})_3$ are EPR silent. We note that this result and the presence of a spectrum for the Er^{3+} complexes is consistent with the EPR spectra of the lanthanide ethylsulfate complexes and anhydrous chloride complexes, which also possess C_{3h} symmetry.[63] In contrast to the Er^{3+} and U^{3+} complexes, all the other compounds have strong axial anisotropy, which can be rationalized by the change in the ordering of the ^{1}H NMR resonances in the Er^{3+} compounds relative to the other lanthanides, as discussed below.

The resulting spectra and corresponding simulations are given in Figure 6 for both U^{3+} complexes. From the extracted *g*-values, the ground-state magnetic moment for each compound

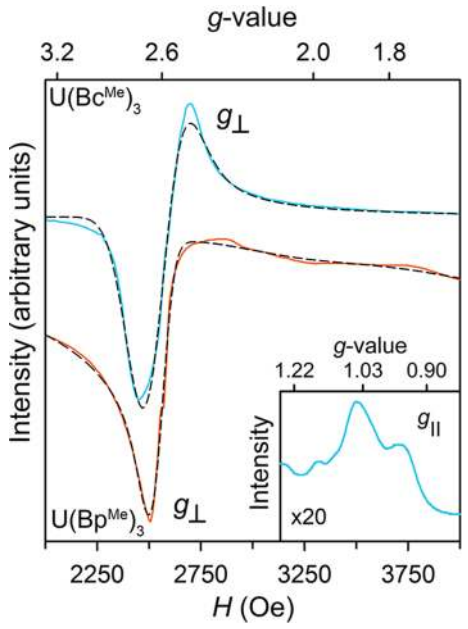

Figure 6. X-band EPR spectra of microcrystalline powder samples of $U(Bc^{Me})_3$ (blue lines) and $U(Bp^{Me})_3$ (orange line) collected at 1.8 K with a microwave frequency of 9.2175 GHz, power of 10 mW, and a modulation amplitude of 1 G. Dashed black lines correspond to simulations of the data, resulting in values of $g_\perp/g_\parallel$ = 2.57/1.03 for $U(Bc^{Me})_3$ and 2.62/1.76 for $U(Bp^{Me})_3$.

was calculated using eq 3 and compared to the moment determined from the magnetic susceptibility, $\chi_M T$, extrapolated to zero K using eq 4.

$$\mu_{eff}^{\ 2} = ({g_1}^2 + {g_2}^2 + {g_3}^3)/4 \quad (3)$$

$$\mu_{eff}^{\ 2} = 7.997 \cdot (\chi_M T)_{(T=0)} \quad (4)$$

This analysis gives μ_{eff} = 2.05 and 1.89 μ_B for $U(Bp^{Me})_3$ and $U(Bc^{Me})_3$, respectively, which are in very good agreement with the values of 2.07(1) μ_B and 1.92(2) μ_B determined from the magnetic susceptibility measurements.[64]

The compounds $U(Bp^{Me})_3$ and $U(Bc^{Me})_3$ possess similar values of $g_\perp$ = 2.62 and 2.57, respectively, revealing a large transverse contribution to the anisotropy. The observation of slow magnetic relaxation only under an applied dc field can thus be understood as arising from tunneling of the magnetization facilitated by the large transverse anisotropy. Despite similar $g_\perp$ values, however, $U(Bc^{Me})_3$ is more anisotropic than $U(Bp^{Me})_3$ with a smaller $g_\parallel$ = 1.03 (compared to $g_\parallel$ = 1.76). This difference suggests that the much slower relaxation observed for $U(Bc^{Me})_3$ is a result of greater magnetic anisotropy, as also proposed below for the lanthanide compounds.

The idealized symmetry for the trigonal prismatic coordination geometry of both compounds is C_{3h}. The behavior of Nd^{3+} in C_{3h} symmetry has been extensively studied,[65,66] and can be applied to the behavior of $U(Bc^{Me})_3$ and $U(Bp^{Me})_3$ to determine the magnetic ground state for these compounds. As noted above, a C_{3h} crystal field will split the $^4I_{9/2}$ ground state of U^{3+} into M_J states of $^5/_2$, $^{-7}/_2$; $^1/_2$; and $^9/_2$, $^{-3}/_2$, although only the first two states satisfy the EPR selection rule ($\Delta M_J = \pm 1$). The *g*-values for the $^1/_2$ state[63,67] are $g_\parallel$ = 0.73 and $g_\perp$ = 3.65, which do not match well with the experimentally observed values.[68] On the other hand, the $^5/_2$, $^{-7}/_2$ state

dx.doi.org/10.1021/ja501569t | J. Am. Chem. Soc. 2014, 136, 6056−6068

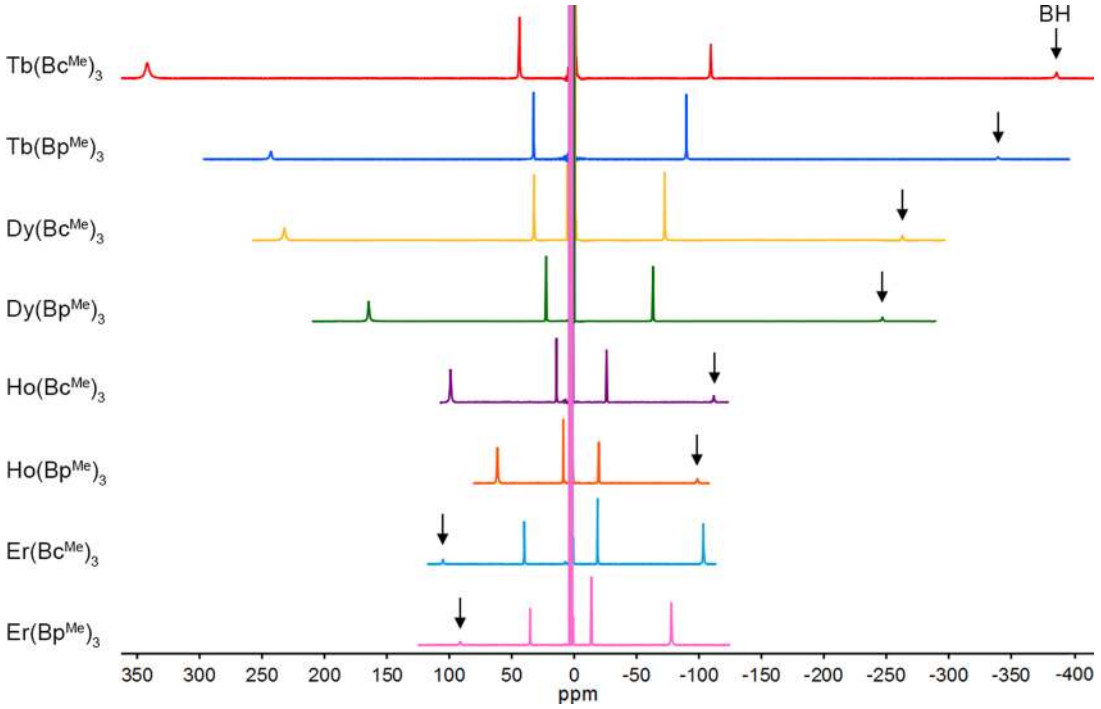

Figure 7. ^{1}H NMR spectra for Ln(Bc^{Me})$_3$ and Ln(Bp^{Me})$_3$ demonstrating much larger chemical shift values for Ln(Bc^{Me})$_3$, which are likely due to a greater dipolar contribution to the chemical shift for this series of compounds.

provides good, but not exact, agreement with the observed *g*-values (see Table S18 in SI). For U(Bc^{Me})$_3$, this agreement is improved by allowing the symmetry to decrease to C_3,[69] therefore allowing the $^{-1}/_2$ state to mix with the $^{5}/_2$, $^{-7}/_2$ state. The same lowering of the symmetry does not improve the agreement for U(Bp^{Me})$_3$.[70] Nevertheless, both complexes possess a ground state that is largely composed of $M_J = {}^{5}/_2$. A similar result has been demonstrated previously using an effective point charge model to simulate magnetic susceptibility data for other U^{3+} scorpionate-based compounds.[11]

^{1}H NMR Spectroscopy. While paramagnetic transition metal complexes often possess long electron spin−lattice relaxation times leading to difficulty in the interpretation of their NMR spectra, this is not the case for the lanthanides. Indeed, large spin−orbit coupling contributes to short relaxation times, and thus peaks can often be readily observed and assigned.[71] The chemical shift of a given nucleus in a paramagnetic complex can be broken down into dipolar (or pseudocontact) and contact contributions. The former is a through-space interaction and arises from coupling of the nuclear and electronic magnetic moments, while the contact (or Fermi contact) shift arises as a consequence of delocalization of unpaired electron spin density from the metal center. In magnetically anisotropic systems, the dipolar contribution is especially important and may be a useful metric in evaluating magnetic anisotropy in isostructural compounds.[72] Room-temperature ^{1}H NMR spectra were collected for M(Bc^{Me})$_3$ and M(Bp^{Me})$_3$ in THF-d_8. In the case of the paramagnetic lanthanides, all complexes demonstrate broad peaks over a wide range of chemical shifts, from −400 to +400 ppm (Figure 7). The spectra possess four peaks each, suggesting that the solid-state structure is maintained in solution, although only one chemical shift is observed due to the borate hydrogen(s).[73] Integration of the Ho(Bp^{Me})$_3$ and Er(Bp^{Me})$_3$ spectra enabled assignments of all observed peaks. Incident protons appear in the same regions of spectral space for the Tb^{3+}, Dy^{3+}, and Ho^{3+} compounds, such that the borate proton(s) are most upfield while the methyl protons are most downfield. This order is reversed for Er^{3+}, however, where the borate proton is now furthest downfield, and the methyl protons furthest upfield. This reversal is due to the presence of dominant transverse anisotropy, as confirmed by EPR spectroscopy, in contrast to the axial anisotropy of the other compounds.[71,72]

The most notable difference is found when comparing spectra for a given metal, wherein the chemical shift for all protons is greater for Ln(Bc^{Me})$_3$ than Ln(Bp^{Me})$_3$. For instance, in the case of Tb(Bc^{Me})$_3$ the methyl proton resonance appears at 340 ppm, while in Tb(Bp^{Me})$_3$ the same resonance is shifted upfield by nearly 100 ppm. Notably, this effect is pronounced for the methyl and borate protons though not as significant for the aromatic protons (Figure S54 in SI). A dominant dipolar contribution to the chemical shift is especially common in the case of the highly anisotropic lanthanides, where contact contributions arising from covalency are generally expected to be small. In this respect, the XANES results indeed suggest that differences between Ln(Bc^{Me})$_3$ and Ln(Bp^{Me})$_3$ are minimal. Thus, the greater chemical shifts for the protons in Ln(Bc^{Me})$_3$ can be interpreted as arising from a greater dipolar contribution compared to Ln(Bp^{Me})$_3$. Given that the dipolar fields experienced by the protons depend heavily on the orientation of the magnetic moment of the molecule, this observation can be interpreted further as evidence of greater magnetic anisotropy in Ln(Bc^{Me})$_3$. Such a hypothesis thus helps to rationalize the differences in magnetic relaxation between Ln(Bc^{Me})$_3$ and Ln(Bp^{Me})$_3$, as a greater preference for the orientation of the magnetic moment in Ln(Bc^{Me})$_3$ should afford larger relaxation barriers and slower relaxation.

For U(Bc^{Me})$_3$ and U(Bp^{Me})$_3$, three ^{1}H NMR peaks integrating in an approximate 2:2:6 ratio appear between zero

dx.doi.org/10.1021/ja501569t | J. Am. Chem. Soc. 2014, 136, 6056−6068

and 14 ppm (Figure S55 in SI), assigned to the aromatic and methyl protons, respectively, suggesting again that the solid-state structure is maintained in solution. Two more broad resonances are also observed in each spectrum with integration values close to 1, which we have assigned to the borate protons in each compound. Relative to the methyl protons in the corresponding diamagnetic Y^{3+} spectra, the methyl peak for $U(Bc^{Me})_3$ is shifted downfield, while that for $U(Bp^{Me})_3$ is shifted upfield. While analysis of the spectra and assessment of magnetic anisotropy magnitude is complicated due to disparity in chemical shifts, the relative positions of the methyl protons might be attributed to opposing signs of the dipolar contribution to the chemical shift.[72]

CONCLUSIONS AND OUTLOOK

Two series of isostructural compounds $M(Bc^{Me})_3$ and $M(Bp^{Me})_3$ have been synthesized with the f-elements Tb, Dy, Ho, Er, and U and fully characterized to examine how donor strength influences slow magnetic relaxation. From dynamic magnetic susceptibility measurements, the presence of a strongly donating *N*-heterocyclic carbene ligand in $M(Bc^{Me})_3$ has been shown to be advantageous in the promotion of slow magnetic relaxation for compounds of the oblate ions U^{3+}, Tb^{3+}, and Dy^{3+} when compared with $M(Bp^{Me})_3$. Interestingly, static magnetic susceptibility characterization of both U^{3+} complexes suggests greater covalency in the case of the *N*-heterocyclic carbene species. Additional characterization utilizing lanthanide $M_{5,4}$-edge XANES, EPR, and ^1H NMR spectroscopies reveals that differences in covalency between the two sets of lanthanide compounds are not as significant. Rather, the *N*-heterocyclic carbene ligand promotes greater magnetic anisotropy for the complexes $M(Bc^{Me})_3$ and therefore slower magnetic relaxation. Furthermore, in both concentrated and dilute samples of $M(Bc^{Me})_3$, the dominant relaxation occurs via an Orbach process, in contrast to $M(Bp^{Me})_3$ for which direct and Raman mechanisms are largely operative. These results ultimately reveal that for uranium and even the lanthanides, donor type and strength are factors of import in the design of new single-molecule magnets. Although relatively short relaxation times and small anisotropy barriers characterize the slowly relaxing systems presented here, the conclusions reached can be applied to further systems demonstrating relaxation under zero field through the exploitation of a more strongly donating ligand field of appropriate symmetry.

ASSOCIATED CONTENT

Supporting Information

Additional magnetic, structural, and spectroscopic characterization data. This material is available free of charge via the Internet at http://pubs.acs.org.

AUTHOR INFORMATION

Corresponding Author

jrlong@berkeley.edu

Notes

The authors declare no competing financial interest.

ACKNOWLEDGMENTS

We thank the NSF Graduate Fellowship Program for support of K.R.M, Prof. R. A. Andersen for valuable discussions, Dr. A. DiPasquale for X-ray structure assistance, and McDonald's Corporation for the drinking straws employed in magnetic sample loading. This research was supported by NSF Grant CHE-1111900. XANES studies were supported under the Heavy Element Chemistry Program at LANL by the Division of Chemical Sciences, Geosciences, and Biosciences, Office of Basic Energy Sciences, U.S. Department of Energy, and at LBNL by the Director, Office of Science, Office of Basic Energy Sciences, Division of Chemical Sciences, Geosciences, and Biosciences of the U.S. Department of Energy (Contract DE-AC02-05CH11231). The Molecular Environmental Science Beamline 11.0.2 at the Advanced Light Source was supported by the Director, Office of Science, Office of Basic Energy Sciences Division of Chemical Sciences, Geosciences, and Biosciences; and the Condensed Phase and Interfacial Molecular Sciences Program of the aforementioned Division of the U.S. Department of Energy at LBNL under Contract No. DE-AC02-05CH11231. The Advanced Light Source is supported by the Director, Office of Science, Office of Basic Energy Sciences, of the U.S. Department of Energy under Contract No. DE-AC02-05CH11231. Los Alamos National Laboratory is operated by Los Alamos National Security, LLC, for the National Nuclear Security Administration of U.S. Department of Energy (Contract DE-AC52-06NA25396).

REFERENCES

(1) Ishikawa, N.; Sugita, M.; Ishikawa, T.; Koshihara, S.-y.; Kaizu, Y. *J. Am .Chem. Soc.* **2003**, *125*, 8694.

(2) Woodruff, D. N.; Winpenny, R. E.; Layfield, R. A. *Chem. Rev.* **2013**, *113*, 5110.

(3) (a) Rinehart, J. D.; Long, J. R. *J. Am. Chem. Soc.* **2009**, *131*, 12558. (b) Magnani, N.; Colineau, E.; Eloirdi, R.; Griveau, J.-C.; Caciuffo, R.; Cornet, S. M.; May, I.; Sharrad, C. A.; Collison, D.; Winpenny, R. E. P. *Phys. Rev. Lett.* **2010**, *104*, 197202. (c) Rinehart, J. D.; Meihaus, K. R.; Long, J. R. *J. Am. Chem. Soc.* **2010**, *132*, 7572. (d) Magnani, M.; Apostolidis, C.; Morgenstern, A.; Colineau, E.; Griveau, J.-C.; Bolvin, H.; Walter, O.; Caciuffo, R. *Angew. Chem., Int. Ed.* **2011**, *50*, 1696. (e) Atunes, M. A.; Pereira, L. C. J.; Santos, I. C.; Mazzanti, M.; Marçalo, J.; Almeida, M. *Inorg. Chem.* **2011**, *50*, 9915. (f) Mills, D. P.; Moro, F.; McMaster, J.; van Slageren, J.; Lewis, W.; Blake, A. J.; Liddle, S. T. *Nat. Chem.* **2011**, *3*, 454. (g) Coutinho, J. T.; Antunes, M. A.; Pereira, L. C. J.; Bolvin, H.; Marcalo, J.; Mazzanti, M.; Almeida, M. *Dalton Trans.* **2012**, *41*, 13568. (h) Mougel, V.; Chatelain, L.; Pecaut, J.; Caciuffo, R.; Colineau, E.; Griveau, J.-C.; Mazzanti, M. *Nat. Chem.* **2012**, *4*, 1011. (i) Rinehart, J. D.; Long, J. R. *Dalton Trans.* **2012**, *41*, 13572. (j) King, D. M.; Tuna, F.; McMaster, J.; Lewis, W.; Blake, A. J.; McInnes, E. J. L.; Liddle, S. T. *Angew. Chem., Int. Ed.* **2013**, *52*, 4921. (k) Moro, F.; Mills, D. P.; Liddle, S. T.; van Slageren, J. *Angew. Chem., Int. Ed.* **2013**, *52*, 3430.

(4) (a) Rinehart, J. D.; Fang, M.; Evans, W. J.; Long, J. R. *Nat. Chem.* **2011**, *3*, 538. (b) Rinehart, J. D.; Fang, M.; Evans, W. J.; Long, J. R. *J. Am. Chem. Soc.* **2011**, *133*, 14236. (c) Demir, S.; Zadrozny, J. M.; Nippe, M.; Long, J. R. *J. Am. Chem. Soc.* **2012**, *134*, 18546.

(5) (a) Guo, Y.-N.; Xu, G.-F.; Wernsdorfer, W.; Ungur, L.; Guo, Y.; Tang, J.; Zhang, H.-J.; Chibotaru, L. F.; Powell, A. K. *J. Am. Chem. Soc.* **2011**, *133*, 11948. (b) Katoh, K.; Kajiwara, T.; Nakano, M.; Nakazawa, Y.; Wernsdorfer, W.; Ishikawa, N.; Breedlove, B. K.; Yamashita, M. *Chem.—Eur. J.* **2011**, *17*, 117. (c) Katoh, K.; Horii, Y.; Yasuda, N.; Wernsdorfer, W.; Toriumi, K.; Breedlove, B. K.; Yamashita, M. *Dalton Trans.* **2012**, *41*, 13582. (d) Tuna, F.; Smith, C. A.; Bodensteiner, M.; Ungur, L.; Chibotaru, L. F.; McInnes, E. J. L.; Winpenny, R. E. P.; Collison, D.; Layfield, R. A. *Angew. Chem., Int. Ed.* **2012**, *51*, 6976. (e) Yi, X.; Bernot, K.; Pointillart, F.; Poneti, G.; Calvez, G.; Daiguebonne, C.; Guillou, O.; Sessoli, R. *Chem.—Eur. J.* **2012**, *18*, 11379. (f) Habib, F.; Brunet, G.; Vieru, V.; Korobkov, I.; Chibotaru, L. F.; Murugesu, M. *J. Am. Chem. Soc.* **2013**, *135*, 13242.

(6) (a) Blagg, R. J.; Muryn, C. A.; McInnes, E. J. L.; Tuna, F.; Winpenny, R. E. P. *Angew. Chem., Int. Ed.* **2011**, *50*, 6530. (b) Blagg, R. J.; Ungur, L.; Tuna, F.; Speak, J.; Comar, P.; Collison, D.;

Wernsdorfer, W.; McInnes, E. J. L.; Chibotaru, L. F.; Winpenny, R. E. P. *Nat. Chem.* **2013**, *5*, 673.
(7) (a) Rinehart, J. D.; Long, J. R. *Chem. Sci.* **2011**, *2*, 2078. (b) Jiang, S.-D.; Wang, B.-W.; Sun, H.-L.; Wang, Z.-M.; Gao, S. *J. Am. Chem. Soc.* **2011**, *133*, 4730. (c) Baldoví, J. J.; Cardona-Serra, S.; Clemente-Juan, J. M.; Coronado, E.; Gaita-Ariño, A.; Palii, A. *Inorg. Chem.* **2012**, *51*, 12565. (d) Chilton, N. F.; Langley, S. K.; Moubaraki, B.; Soncini, A.; Batten, S. R.; Murray, K. S. *Chem. Sci.* **2013**, *4*, 1719. (e) Chilton, N. F.; Collison, D.; McInnes, E. J. L.; Winpenny, R. E. P.; Soncini, A. *Nat. Commun.* **2013**, *4*, 2551.
(8) (a) Ungur, L.; Chibotaru, L. F. *Phys. Chem. Chem. Phys.* **2011**, *13*, 20086. (b) Liu, J.-L.; Chen, Y.-C.; Zheng, Y.-Z.; Lin, W.-Q.; Ungur, L.; Wernsdorfer, W.; Chibotaru, L. F.; Tong, M.-L. *Chem. Sci.* **2013**, *4*, 3310. (c) Boulon, M.-E.; Cucinotta, G.; Liu, S.-S.; Jiang, S.-D.; Ungur, L.; Chibotaru, L. F.; Gao, S.; Sessoli, R. *Chem.—Eur. J.* **2013**, *19*, 13726.
(9) (a) da Cunha, T. T.; Jung, J.; Boulon, M.-E.; Campo, G.; Pointillart, F.; Pereira, C. L. M.; Le Guennic, B.; Cador, O.; Bernot, K.; Pineider, F.; Golhen, S.; Ouahab, L. *J. Am. Chem. Soc.* **2013**, *135*, 16332. (b) Boulon, M.-E.; Cucinotta, G.; Luzon, J.; Degl'Innocenti, C.; Perfetti, M.; Bernot, K.; Calvez, G.; Caneschi, A.; Sessoli, R. *Angew. Chem., Int. Ed.* **2013**, *52*, 350.
(10) Baldoví, J. J.; Borrás-Almenar, J. J.; Clemente-Juan, J. M.; Coronado, E.; Gaita-Ariño, A. *Dalton Trans.* **2012**, *41*, 13705.
(11) Baldoví, J. J.; Cardona-Serra, S.; Clemente-Juan, J. M.; Coronado, E.; Gaita-Ariño, A. *Chem. Sci.* **2013**, *4*, 938.
(12) (a) Lukens, W. W.; Edelstein, N. M.; Magnani, N.; Hayton, T. W.; Fortier, S.; Seaman, L. *J. Am. Chem. Soc.* **2013**, *135*, 10742. (b) Behrle, A. C.; Barnes, C. L.; Kaltsoyannis, N.; Walensky, J. R. *Inorg. Chem.* **2013**, *52*, 10623. (c) Neidig, M. L.; Clark, D. L.; Martin, R. L. *Coord. Chem. Rev.* **2013**, *257*, 394. (d) Minasian, S. G.; Keith, J. M.; Batista, E. R.; Boland, K. S.; Clark, D. L.; Kozimor, S. A.; Martin, R. L.; Shuh, D. K.; Tyliszczak, T. *Chem. Sci.* **2014**, *5*, 351 and references therein.
(13) Meihaus, K. R.; Rinehart, J. D.; Long, J. R. *Inorg. Chem.* **2011**, *50*, 8484.
(14) (a) Jeletic, M.; Lin, P.-H.; Le Roy, J. J.; Korobkov, I.; Gorelsky, S. I.; Murugesu, M. *J. Am. Chem. Soc.* **2011**, *133*, 19286. (b) Le Roy, J. J.; Jeletic, M.; Gorelsky, S. I.; Korobkov, I.; Ungur, L.; Chibotaru, L. F.; Murugesu, M. *J. Am. Chem. Soc.* **2013**, *135*, 3502. (c) Meihaus, K.; Long, J. R. *J. Am. Chem. Soc.* **2013**, *135*, 17952.
(15) Smith, J. M. *Comments Inorg. Chem.* **2008**, *29*, 189.
(16) Cloke, F. G. N.; Hitchcock, P. B. *J. Am. Chem. Soc.* **2002**, *124*, 9352.
(17) Spedding, F. H.; Newton, A. S.; Warf, J. C.; Johnson, O.; Nottorf, R. W.; Johns, I. B.; Daane, A. H. *Nucleonics* **1949**, *4*, 4.
(18) Munguia, T.; Bakir, Z. A.; Cervantes-Lee, F.; Metta-Magana, A.; Pannell, K. H. *Organometallics* **2009**, *28*, 5777.
(19) Niedenzu, K.; Niedenzu, P. M.; Warner, K. R. *Inorg. Chem.* **1985**, *24*, 1604.
(20) Fränkel, R.; Kniczek, J.; Ponikwar, W.; Nöth, H.; Polborn, K.; Fehlhammer, W. P. *Inorg. Chim. Acta* **2001**, *312*, 23.
(21) Nieto, I.; Bontchev, R. P.; Smith, J. M. *Eur. J. Inorg. Chem.* **2008**, 2476.
(22) Assuming the presence of no organic impurities, using the crystalline solid isolated directly from the reaction of $[H_2B(MeIm)_2]I$ and LDA, a starting amount of metal reagent was chosen to be one-third of the molar amount of theoretical $Li[Bc^{Me}]$ present.
(23) Burla, M. C.; Caliandro, R.; Camalli, M.; Carrozzini, B.; Cascarano, G. L.; De Caro, L.; Giacovazzo, C.; Polidori, G.; Spagna, R. *J. Appl. Crystallogr.* **2005**, *38*, 381.
(24) Sheldrick, G. M. *Acta Crystallogr.* **2008**, *A64*, 112.
(25) Bain, G. A.; Berry, J. F. *J. Chem. Educ.* **2008**, *85*, 532.
(26) Gatteschi, D.; Sessoli, R.; Villain, J. *Molecular Nanomagnets*; Oxford University Press: Oxford, 2006.
(27) Daul, C.; Schlapfer, C. W.; Mohos, B.; Ammeter, J.; Gamp, E. *Comput. Phys. Commun.* **1981**, *21*, 385.
(28) Pilbrow, J. R. *Transition Ion Electron Paramagnetic Resonance*; Clarendon Press: Oxford, 1990.
(29) Gasgnier, M.; Schiffmacher, G.; Albert, L.; Caro, P. E.; Dexpert, H.; Esteva, J. M.; Blancard, C.; Karnatak, R. C. *J. Less-Common Met.* **1989**, *156*, 59.
(30) (a) Bugaris, D. E.; Choi, E. S.; Copping, R.; Glans, P.-A.; Minasian, S. G.; Tyliszczak, T.; Kozimor, S. A.; Shuh, D. K.; Ibers, J. A. *Inorg. Chem.* **2011**, *50*, 6656. (b) Gianetti, T. L.; Nocton, G.; Minasian, S. G.; Tomson, N. C.; Kilcoyne, A. L. D.; Kozimor, S. A.; Shuh, D. K.; Tyliszczak, T.; Bergman, R. G.; Arnold, J. *J. Am. Chem. Soc.* **2013**, *135*, 3224. (c) Minasian, S. G.; Keith, J. M.; Batista, E. R.; Boland, K. S.; Bradley, J. A.; Daly, S. R.; Kozimor, S. A.; Lukens, W. W.; Martin, R. L.; Nordlund, D.; Seidler, G. T.; Shuh, D. K.; Sokaras, D.; Tyliszczak, T.; Wagner, G. L.; Weng, T.-C.; Yang, P. *J. Am. Chem. Soc.* **2013**, *135*, 1864.
(31) Bluhm, H.; Andersson, K.; Araki, T.; Benzerara, K.; Brown, G. E.; Dynes, J. J.; Ghosal, S.; Gilles, M. K.; Hansen, H.-Ch; Hemminger, J. C.; Hitchcock, A. P.; Ketteler, G.; Kilcoyne, A. L. D.; Kneedler, E.; Lawrence, J. R.; Leppard, G. G.; Majzlam, J.; Mun, B. S.; Myneni, S. C. B.; Nilsson, A.; Ogasawara, H.; Ogletree, D. F.; Pecher, K.; Salmeron, M.; Shuh, D. K.; Tonner, B.; Tyliszczak, T.; Warwick, T.; Yoon, T. H. *J. Electron Spectrosc. Relat. Phenom.* **2006**, *150*, 86.
(32) (a) Nieto, I.; Ding, F.; Bontchev, R. P.; Wang, H.; Smith, J. M. *J. Am. Chem. Soc.* **2008**, *130*, 2716. (b) Scepaniak, J. J.; Fulton, M. D.; Bontchev, R. P.; Duesler, E. N.; Kirk, M. L.; Smith, J. M. *J. Am. Chem. Soc.* **2008**, *130*, 10515. (c) Scepaniak, J. J.; Young, J. A.; Bontchev, R. P.; Smith, J. M. *Angew. Chem., Int. Ed.* **2009**, *48*, 3158. (d) Scepaniak, J. J.; Vogel, C. S.; Khusniyarov, M. M.; Heinemann, F. W.; Meyer, K.; Smith, J. M. *Science* **2011**, *331*, 1049. (e) Li, S.; Wang, Z.; Hor, T. S. A.; Zhao, J. *Dalton Trans.* **2012**, *41*, 1454.
(33) (a) Grubbs, R. H. *Angew. Chem., Int. Ed.* **2006**, *45*, 3760. (b) Bantreil, X.; Broggi, J.; Nolan, S. P. *Annu. Rep. Prog. Chem., Sect. B: Org. Chem.* **2009**, *105*, 232. (c) Fortman, G. C.; Nolan, S. P. *Chem. Soc. Rev.* **2011**, *40*, 5151.
(34) (a) Mehdoui, T.; Berthet, J.-C.; Thuéry, P.; Ephritikhine, M. *Chem. Commun.* **2005**, 2860. (b) Arnold, P. L.; Turner, Z. R.; Germeroth, A. I.; Casely, I. J.; Bellabarba, R.; Tooze, R. P. *Dalton Trans.* **2010**, *39*, 6808.
(35) (a) Arnold, P. L.; Liddle, S. T. *Chem Comm.* **2006**, 3959 and references therein. (b) Arnold, P. L.; Casely, I. J.; Turner, Z. R.; Carmichael, C. D. *Angew. Chem., Int. Ed.* **2008**, *14*, 10415.
(36) Schettini, M. F.; Wu, G.; Hayton, T. W. *Chem. Commun.* **2012**, *48*, 1484.
(37) Rai, S. B. *Spectrochim. Acta, Part A* **2002**, *58*, 1559.
(38) (a) Carvalho, A.; Domingos, A.; Gaspar, P.; Marques, N.; Pires de Matos, A.; Santos, I. *Polyhedron* **1992**, *11*, 1481. (b) Sun, Y.; Takats, J.; Eberspacher, T.; Day, V. *Inorg. Chim. Acta* **1995**, *229*, 315. (c) Sessler, J. L.; Melfi, P. J.; Pantos, G. D. *Coord. Chem. Rev.* **2006**, *250*, 816. (d) Pettinari, C. *Scorpionates II: Chelating Borate Ligands*; Imperial College Press: London, 2008. (e) Tsoureas, N.; Nunn, J.; Bevis, T.; Haddow, M. F.; Hamilton, A.; Owen, G. R. *Dalton Trans.* **2011**, *40*, 951.
(39) Raymond, K. N.; Eigenbrot, C. W. *Acc. Chem. Res.* **1980**, *13*, 276.
(40) Kepert, D. L. *Inorganic Stereochemistry*; Springer-Verlag Berlin: Heidelberg, 1982.
(41) van Vleck, J. H. *The Theory of Electric and Magnetic Susceptibilities*; Oxford University Press: London, 1932.
(42) The small slope can be ascribed to TIP due to mixing of the $J = {}^{11}/_{2}$ state into the $J = {}^{9}/_{2}$ ground state by the crystal field.
(43) Stevens, K. W. H. *Proc. R. Soc. A.* **1953**, *219*, 542.
(44) Kahn, O. *Molecular Magnetism*; Wiley-VCH: New York, 1993.
(45) (a) Gatteschi, D.; Sessoli, R. *Angew. Chem., Int. Ed.* **2003**, *42*, 268. (b) Sessoli, R.; Powell, A. K. *Coord. Chem. Rev.* **2009**, *253*, 2328.
(46) A low frequency rise is observed for both complexes at 1.8 K and applied fields. However, this signal appears to be intermolecular in origin, as this tail rapidly goes to zero with increase in temperature.
(47) The temperature-dependence of the relaxation time is $\tau \propto T^n$, where $n = 9$ (7) if the metal ion is Kramers (non-Kramers). $\tau \propto T^S$ is also sometimes observed for Kramers ions (see for example ref 7and Yersin, H.; Strasser, J. *Coord. Chem. Rev.* **2000**, *208*, 331.

(48) For a direct process, typically $\tau \propto T$; however, $\tau \propto T^2$, a so-called bottleneck direct process, is also possible.
(49) (a) Harman, W. H.; Harris, T. D.; Freedman, D. E.; Fong, H.; Chang, A.; Rinehart, J. D.; Ozarowski, A.; Sougrati, M. T.; Grandjean, F.; Long, G. J.; Long, J. R.; Chang, C. J. *J. Am. Chem. Soc.* **2010**, *132*, 18115. (b) Zadrozny, J. M.; Atanasov, M.; Bryan, A. M.; Lin, C.-Y.; Rekken, B. D.; Power, P. P.; Neese, F.; Long, J. R. *Chem. Sci.* **2013**, *4*, 125.
(50) Raman and direct relaxation processes have been identified in a Dy^{3+} tetramer: (a) Guo, Y.-N.; Xu, G.-F.; Gamez, P.; Zhao, L.; Lin, S.-Y.; Deng, R.; Tang, J.; Zhang, H.-J. *J. Am. Chem. Soc.* **2010**, *132*, 8538 though the full range of thermally-dependent relaxation data was not simultaneously fit accounting for all these processes. More recently, a comprehensive study on the effect of ligand functionalization on slow relaxation for Er^{3+} presented evidence for the dominance of a Raman process for variously functionalized complexes of the trensal^{3-} ligand (H_3trensal = 2,2′,2″-tris(salicylideneimino)triethylamine). (b) Pedersen, K. S.; Ungur, L.; Sigrist, M.; Sundt, A.; Schau-Magnussen, M.; Vieru, V.; Mutka, H.; Rols, S.; Weihe, H.; Waldmann, O.; Chibotaru, L. F.; Bendix, J.; Dreiser, J. *Chem. Sci.* **2014**, *5*, 1650.
(51) This explicit equation was first used to fit field-dependent relaxation data for some $LnCl_3$ in: Bohan, T. L.; Stapleton, H. J. *Phys. Rev.* **1969**, *182*, 385.
(52) For all uranium samples, a Raman exponent $m = 5$ was found to give a better fit than $m = 9$. A T^5 temperature dependence has been rationalized by Orbach for a multi-level Kramers system in which Raman relaxation occurs between two states that are not time-reversed Kramers states. See Orbach, R.; Blume, M. *Phys. Rev. Lett.* **1962**, *8*, 478.
(53) This process goes away with dilution, suggesting that it is of dipolar origin.
(54) While Ho^{3+} might also be considered an "oblate" ion, the 100% abundant $I = {}^7/_2$ nuclear spin could contribute to very fast relaxation and hence the lack of slow relaxation observed for $Ho(Bc^{Me})_3$ or $Ho(Bp^{Me})_3$.
(55) (a) Fuggle, J. C.; Hillebrecht, F. U.; Esteva, J. M.; Karnatak, R. C.; Gunnarsson, O.; Schonhammer, K. *Phys. Rev. B* **1983**, *27*, 4637. (b) Bradley, J. A.; Moore, K. T.; Lipp, M. J.; Mattern, B. A.; Pacold, J. I.; Seidler, G. T.; Chow, P.; Rod, E.; Xiao, Y.; Evans, W. J. *Phys. Rev. B* **2012**, *85*, 100102. (c) Hu, Z. W.; Kaindl, G.; Meyer, G. *J. Alloys Compd.* **1997**, *246*, 186. (d) Gordon, R. A.; Seidler, G. T.; Fister, T. T.; Nagle, K. P. *J. Electron Spectrosc. Relat. Phenom.* **2011**, *184*, 220.
(56) (a) Kaindl, G.; Brewer, W. D.; Kalkowski, G.; Holtzberg, F. *Phys. Rev. Lett.* **1983**, *51*, 2056. (b) Bradley, J. A.; Moore, K. T.; van der Laan, G.; Bradley, J. P.; Gordon, R. A. *Phys. Rev. B* **2011**, *84*, 205105.
(57) (a) Thole, B. T.; Vanderlaan, G.; Fuggle, J. C.; Sawtzky, G. A.; Karnatak, R. C.; Esteva, J. M. *Phys. Rev. B* **1985**, *32*, 5107. (b) Thole, B. T.; van der Laan, G. *Phys. Rev. B.* **1988**, *38*, 3158.
(58) (a) Kotani, A.; Ogasawara, H. J. *J. Electron Spectrosc. Relat. Phenom.* **1992**, *60*, 257. (b) Fortner, J. A.; Buck, E. C. *Appl. Phys. Lett.* **1996**, *68*, 3817.
(59) Manoubi, T.; Colliex, C.; Rex, P. *J. Electron Spectrosc. Relat. Phenom.* **1990**, *50*, 1.
(60) (a) Kaindl, G.; Kalkowski, G.; Brewer, W. D.; Perscheid, B.; Holtzberg, F. *J. Appl. Phys.* **1984**, *55*, 1910. (b) Ayala, P.; Kitaura, R.; Nakanishi, R.; Shiozawa, H.; Ogawa, D.; Hoffmann, P.; Shinohara, H.; Pichler, T. *Phys. Rev. B* **2011**, *83*, 085407. (c) Nakamura, T.; Hirono, T.; Kinoshita, T.; Narumi, Y.; Hayashi, M.; Nojiri, H.; Mitsuda, A.; Wada, H.; Kodama, K.; Kindo, K.; Kotani, A. *J. Phys. Soc. Jpn.* **2012**, *81*, 103705.
(61) (a) Karnatak, R. C. *J. Alloys Compd.* **1993**, *192*, 64. (b) Gasgnier, M.; Schiffmacher, G.; Albert, L.; Caro, P. E.; Dexpert, H.; Esteva, J. M.; Blancard, C.; Karnatak, R. C. *J. Less-Common Met.* **1989**, *156*, 59. (c) Gasgnier, M.; Eyring, L.; Karnatak, R. C.; Dexpert, H.; Esteva, J. M.; Caro, P.; Albert, L. *J. Less-Common Met.* **1987**, *127*, 367. (d) Dexpert, H.; Karnatak, R. C.; Esteva, J. M.; Connerade, J. P.; Gasgnier, M.; Caro, P. E.; Albert, L. *Phys. Rev. B* **1987**, *36*, 1750.
(62) Shim, J. H.; Haule, K.; Kotliar, G. *Europhys. Lett.* **2009**, *85*, 17007.
(63) Abragam, A.; Bleaney, B. *Electron Paramagnetic Resonance of Transition Ions*; Clarendon Press: Oxford, 1970.
(64) Extrapolation of the dc susceptibility data for Tb, Dy, and Ho compounds was attempted in the same way, utilizing eqs 3 and 4 and assuming $g_\perp = 0$. However, a small amount of torqueing could not be resolved at low temperature in the Tb data, and small mass uncertainty in the case of all complexes makes such a calculation unreliable in the absence of other supporting data such as EPR. However, the ^{1}H NMR results clearly testify to the presence of axial anisotropy for these complexes, and a greater anisotropy in the case of $M(Bc^{Me})_3$.
(65) Judd, B. R. *Proc. R. Soc. A* **1955**, *232*, 458.
(66) Elliott, R. J.; Stevens, K. W. H. *Proc. R. Soc. A* **1953**, *219*, 387.
(67) Defined as $g_\perp = 5g_\parallel = 5g_J$ (where g_J is the Landé g-value = ${}^8/_{11}$ for f^3).
(68) The agreement may be improved somewhat by including the effect of mixing the ${}^{11}/_2$, ${}^1/_2$ state into the ${}^9/_2$,${}^1/_2$ state by the crystal field; however, here the agreement is still poor.
(69) This symmetry relaxing also more accurately represents the true molecular symmetry of the compound, which lacks a horizontal mirror plane.
(70) It is also possible that mixing of the relevant $J = {}^{11}/_2$ states into the ground state would improve the agreement, but this possibility cannot be examined as the resulting state uses three parameters rather than the single parameter needed for the ${}^5/_2$, ${}^{-7}/_2$ state.
(71) La Mar, G. N.; Horrocks, W. DeW. Jr.; Holm, R. H.. Eds. *NMR of Paramagnetic Molecules; Principles and Applications*; Academic Press: New York, 1973.
(72) Bertini, I.; Luchinat, C. *NMR of Paramagnetic Molecules in Biological Systems*; Benjamin/Cummings Publishing Company, Inc: Menlo Park, 1986.
(73) In the case of the $Er(Bc^{Me})_3$ spectra, as a representative example, the four peaks were found to integrate in a ∼6:2:2:1 ratio (corresponding to the methyl [most upfield] peak, the aromatic [most intense] peaks, and one borate proton [most downfield] resonance, respectively). Thus, we believe that the second borate proton resonance is too broad to be observed on the time-scale of these experiments.